Diagnosing Water Mass Formation from Air–Sea Fluxes and Surface Mixing

A. J. G. NURSER AND ROBERT MARSH

James Rennell Division for Ocean Circulation and Climate, Southampton Oceanography Centre, Southampton, United Kingdom

RICHARD G. WILLIAMS

Oceanography Laboratories, University of Liverpool, Liverpool, United Kingdom

(Manuscript received 7 October 1996, in final form 27 July 1998)

ABSTRACT

The formation rate of water masses and its relation to air–sea fluxes and interior mixing are examined in an isopycnic model of the North (and tropical) Atlantic that includes a mixed layer. The diagnostics follow Walin's formulation, linking volume and potential density budgets for an isopycnal layer.

The authors consider the balance between water mass production, mixing, and air–sea fluxes in the model in the context of two limit cases: (i) with no mixing, where air–sea fluxes drive water mass formation directly, and (ii) a steady state in a closed basin, where air–sea fluxes are balanced by diffusion. In such a steady state, since mixing always acts to *reduce* density contrast, surface forcing must act to *increase* it.

Considered over the whole basin, including the Tropics, the model is in steady state apart from the densest layers. Most of the mixing is achieved by diapycnal diffusion in the strong density gradients within upwelling regions in the Tropics, and by entrainment into the tropical mixed layer. Mixing from entrainment associated with the seasonal cycle of mixed layer depth in mid and high latitudes and lateral mixing of density within the mixed layer are less important than this tropical mixing. These model results as to the relative importance of the different mixing processes are consistent with a simple scaling analysis.

Outside the Tropics, the upwelling-linked mixing is no longer important, and a first-order estimate of water mass formation rates may be made from the surface fluxes. Lateral mixing of density within the mixed layer and seasonal entrainment mixing are as important as the remaining thermocline mixing within this domain.

An apparent vertical diffusivity is diagnosed over both the full and extratropical domain. It reaches 10^{-4} m^2 s^{-1} for the denser waters, about four times as large as the explicit diapycnal diffusion within the thermocline.

1. Introduction

In a pioneering work, Walin (1982) presented a view of the thermal circulation in terms of the flow of water across isotherms being driven by heating and cooling. This work can easily be generalized to link the diapycnal flow and (potential) density fluxes. In this formulation, the rate of formation of a water mass between two isopycnals $M(\rho)$ is given by

$$M(\rho) = -\frac{\partial F}{\partial \rho} + \frac{\partial^2 D_{\text{diff}}}{\partial \rho^2}, \tag{1}$$

where F represents the density input by surface fluxes into the surface outcrop of the ρ isopycnal, and D_{diff} represents the total diapycnal diffusive density flux across it resulting from interior mixing.

In principle, this deceptively simple relation allows the formation rate to be diagnosed from only the diabatic forcing without requiring any additional information about the circulation or dynamics. Speer and Tziperman (1992) have exploited this relation to estimate the formation rate of water masses in the North Atlantic from climatological surface heat and freshwater fluxes, but did not consider interior mixing. Speer (1993) found that the surface fluxes implied core water mass properties consistent with observations of mode waters revealed in the volumetric census of T and S in the classic work by Worthington (1976, 1981). Tziperman and Speer (1994), Speer et al. (1995), and Speer et al. (1997) have similarly applied this algorithm to the Mediterranean, over the whole globe, and to the Southern Ocean, respectively. It has also been applied to the seasonal thermocline and linked to annual-average subduction rates (Tandon and Garrett 1997; Marshall et al. 1998).

Of course, the formation rate is only given by the air–sea fluxes in the absence of interior diabatic mixing. In fact, in a closed basin in a steady state, we know that

Corresponding author address: Dr. A. J. G. Nurser, James Rennell Division for Ocean Circulation and Climate, Southampton Oceanography Centre, Empress Dock, Southampton SO143ZH, United Kingdom.
E-mail: g.nurser@soc.soton.ac.uk

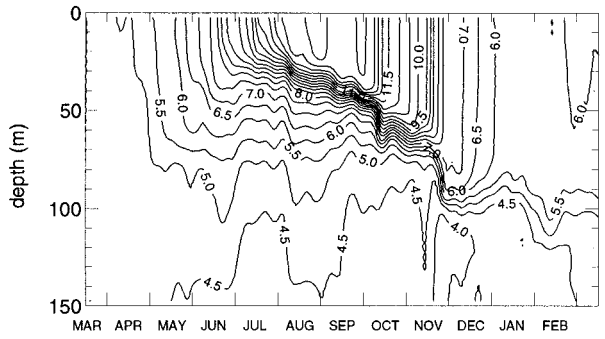

FIG. 1. The annual cycle at OWS Papa (50°N, 145°W) of the depth profile of temperature in °C over the ''ocean year'' 15 March 1961 to 15 March 1962. Redrawn from Large et al. (1994).

the formation rate is zero. Given the surface fluxes, Walin's formalism can thus be used to ''back out'' the diffusive fluxes, and, indeed, Walin (1982) estimated the mean global diapycnal diffusivity in the thermocline in this way. More generally, if we know the water mass production and the surface fluxes, then the diffusion can be diagnosed. For example, Speer (1997) has estimated the mean diapycnal diffusivity in the North Atlantic by comparing climatological surface fluxes north of 11°S in the Atlantic with water mass export across a section at 11°S.

However, it is not clear how meaningful is the ''mean'' diapycnic diffusivity since mixing in the upper-ocean surface boundary layer may be important. Vigorous lateral mixing of density within the mixed layer is driven by eddies in baroclinically unstable regions. This mixing is most likely to be important in the deep winter mixed layers.

There is also enhanced mixing near the base of the surface mixed layer through the action of the wind, penetrative convection, and internal wave breaking (see Large et al. 1994 for a review). In particular, mixing occurs whenever dense thermocline water is entrained into the lighter mixed layer. The importance of this entrainment mixing can be seen, for instance, in the annual cycle of temperature at OWS Papa, a site (50°N, 145°W in the Pacific Ocean) where advection is comparatively weak (Gill and Niiler 1973). In autumn and winter (Fig. 1), even though there is surface heat loss, isotherms in the 5°–7°C range are pushed down as turbulence mixes down heat from the warm mixed layer into the seasonal thermocline. This gives an annual-average heat loss from the mixed layer of the order of 25 W m^{-2} (see section 3b), which can be comparable to the annual surface heat flux. The importance of this mixing driven by seasonal entrainment has been discussed by Garrett and Tandon (1997).

In section 4 of this study, we use Walin's formulation to diagnose the rate of formation of water masses in a numerical isopycnic model of the North Atlantic (Bleck et al. 1992). Using the model allows us to diagnose all the diabatic processes. Unlike the models diagnosed by McWilliams et al. (1996) and Marshall et al. (1998), this model has an explicit mixed layer including turbulent mixing from the wind, and so should give entrainment mixing. We examine how the air–sea fluxes are balanced by the different modes of interior mixing:

1) diapycnal diffusion within the thermocline,
2) lateral mixing within the mixed layer, and the entrainment of dense thermocline water into the lighter surface mixed layer, both
3) as a result of sustained upwelling in equatorial regions, and
4) as a result of autumn/winter deepening of the mixed layer at midlatitudes.

Before the model diagnosis, we rederive in section 2 Walin's relations linking surface and diffusive density fluxes to diapycnal volume fluxes and formation rates. We present two idealized examples, one where surface fluxes drive water mass production and the other where interior diffusive and surface fluxes balance so as to give a steady state. In section 3, we discuss the various mechanisms of mixing and perform a rough scale analysis of their relative importance.

2. Theoretical derivations for water mass formation

a. Walin's relations for formation rate

Walin (1982) derived elegant relations between water mass formation and diffusive and radiative (nonadvective) heat fluxes, combining heat and volume budgets for an isothermal layer. Here, we repeat the derivation of Walin's relations in terms of potential density and illustrate their use with idealized examples. Throughout the paper, when we refer to ''density,'' it should be understood as *potential* density.

1) WATER MASS FORMATION AND DIAPYCNAL VOLUME FLUXES

Consider the volume sandwiched between the isopycnal surfaces with potential densities ρ and $\rho + \Delta\rho$. We consider a limited area of the ocean, such as the North Atlantic, with an open boundary (Fig. 2a).

We first define water mass formation using a volume budget of a density layer. We write

ΔV the volume of fluid with density between ρ and $\rho + \Delta\rho$

$\Delta\Psi$ the volume flux of fluid with density between ρ and $\rho + \Delta\rho$ out of the domain

$G(\rho)$, $G(\rho + \Delta\rho)$ the diapycnal volume flux of fluid crossing the ρ and $\rho + \Delta\rho$ isopycnals respectively; note that Speer and Tziperman (1992) refer to this term as transformation and denote it by A. The sign convention is (see Fig. 2a) that G is positive if directed toward increasing ρ.

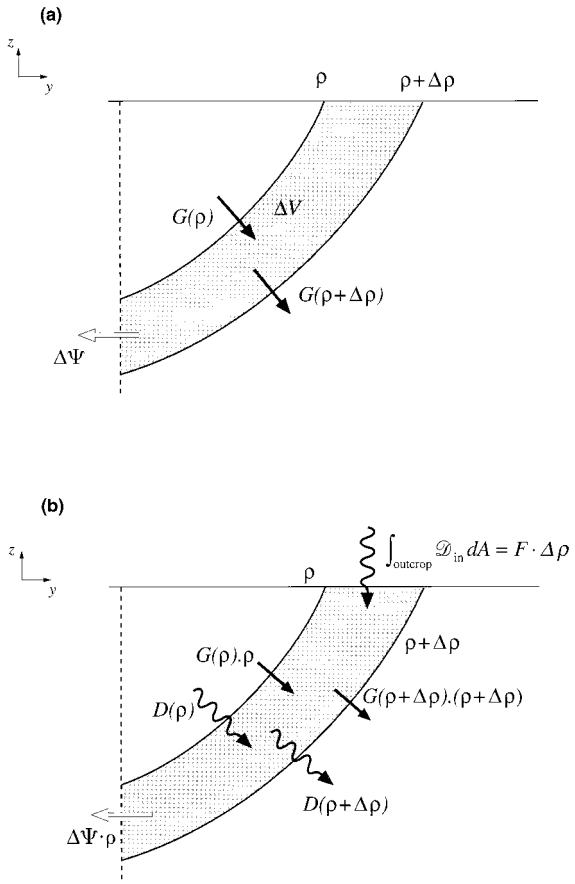

FIG. 2. Schematic vertical sections showing the volume and mass balances for a volume element bounded by the density surfaces ρ and $\rho + \Delta\rho$ that outcrop at the sea surface: (a) the volume of the layer depends on the divergence of the diapycnal volume flux G, crossing the temperature surfaces, and the volume flux exiting the domain $\Delta\Psi$ (b) the mass content of the layer depends on the advective change from the diapycnal volume flux ρG and the mass exiting the domain $\rho\Delta\Psi$, as well as the divergence of the diffusive mass fluxes D_{diff} and the density gained from the atmosphere $\int_{\text{outcrop}} \mathcal{D}_{\text{in}}\, dA = F\Delta\rho$ over the surface outcrop.

We assume incompressibility. Then the volume budget of the control volume bounded by the ρ and $\rho + \Delta\rho$ isopycnals, the ocean surface, and the open boundary is

$$\left(\frac{\partial \Delta V}{\partial t} + \Delta\Psi\right) = G(\rho) - G(\rho + \Delta\rho). \tag{2}$$

Summing the volume inflation and the outflow terms gives the water mass formation

$$M\Delta\rho = \frac{\partial \Delta V}{\partial t} + \Delta\Psi, \tag{3}$$

where the water mass formation per unit of density, M, is given by the convergence of the diapycnal volume flux

$$M = -\frac{\partial G}{\partial \rho}. \tag{4}$$

2) Diapycnal volume fluxes and density sources

We now consider the density budget for the same layer (see Fig. 2b). We write $\mathcal{D}$ as the density flux per unit area and D as the *area-integrated* density flux across an isopycnal, defined to be positive in the direction of increasing density. We then have

$D_{\text{diff}}(\rho)$, $D_{\text{diff}}(\rho + \Delta\rho)$ the integrated diapycnal density flux across the ρ and $\rho + \Delta\rho$ isopycnals, and

$\int_{\text{outcrop}} \mathcal{D}_{\text{in}}\, dA$ the total density flux into the ocean where the surface density lies between ρ and $\rho + \Delta\rho$; here $\mathcal{D}_{\text{in}}$ is the density influx per unit area.

The density budget of the control volume between the ρ and $\rho + \Delta\rho$ isopycnals is a balance between advective and diffusive density fluxes:

$$\underbrace{\left(\frac{\partial(\Delta V)}{\partial t} + \Delta\Psi\right)\rho + (\rho + \Delta\rho)G(\rho + \Delta\rho) - \rho G(\rho)}_{\text{density content gain of layer + outward advective density fluxes}}$$

$$= \underbrace{-(D_{\text{diff}}(\rho + \Delta\rho) - D_{\text{diff}}(\rho)) + \int_{\text{outcrop}} \mathcal{D}_{\text{in}}\, dA,}_{\text{diffusive influx of density}}$$

or more concisely

$$M\rho + \frac{\partial}{\partial \rho}(\rho G) = -\frac{\partial D_{\text{diff}}}{\partial \rho} + F, \tag{5}$$

where we have introduced F, the surface density influx per unit of density (Fig. 2b):

$$F = \lim_{\Delta\rho \to 0} \frac{1}{\Delta\rho} \int_{\text{outcrop}} \mathcal{D}_{\text{in}}\, dA. \tag{6}$$

This F is Speer and Tziperman's (1992) transformation driven by air–sea fluxes.

But by volume conservation (4) $M = -\partial G/\partial\rho$, so the density content gain implicit in volume inflation and lateral outflux may be eliminated in (5), leaving

$$G(\rho) = -\frac{\partial D_{\text{diff}}}{\partial \rho} + F. \tag{7}$$

Thus, a cross-isopycnal volume flux directed from light to dense, $G(\rho) > 0$, requires a density supply either from a convergence of diapycnal density fluxes, $-\partial D_{\text{diff}}/\partial\rho > 0$, or from the surface, $F > 0$. There is, in fact, also an extra density source in (5) arising from cabbeling—densification through mixing—for example, McDougall (1984). This term is generally small and is neglected here for simplicity.

Combining (7) and (4) gives (1)

$$M(\rho) = -\frac{\partial F}{\partial \rho} + \frac{\partial^2 D_{\text{diff}}}{\partial \rho^2}.$$

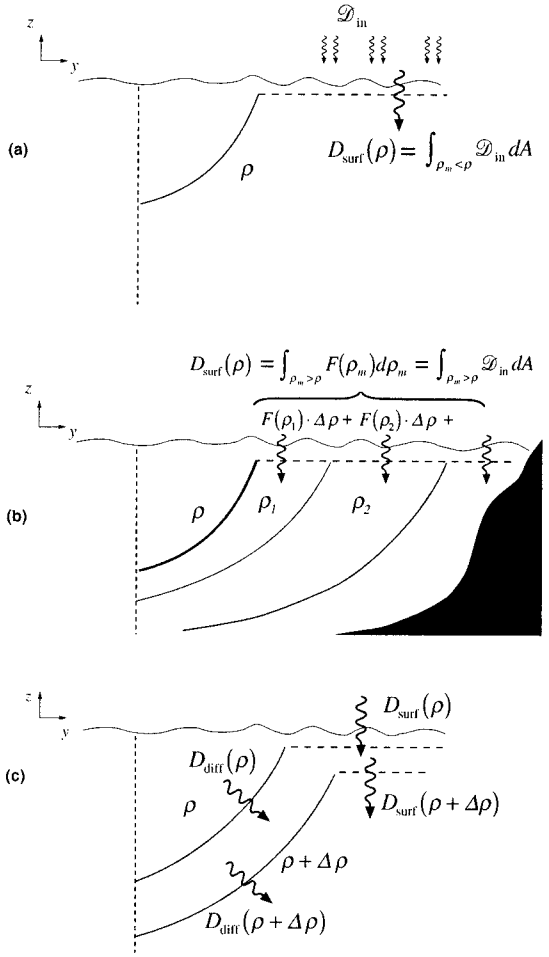

FIG. 3. (a) A schematic vertical section showing the ρ isopycnal (solid line) and its surface extension (dotted line). The surface extension lies along the sea surface wherever the isopycnal is lighter than the surface mixed layer water $\rho < \rho_m(\mathbf{x})$. The density flux through the surface extension is then $D_{\rm surf} = \int_{\rho_m>\rho} \mathcal{D}_{\rm in}\, dA$. (b) The density flux $D_{\rm surf}(\rho)$ through the surface extension is made up of the surface fluxes F into all the outcropping isopycnals denser than ρ. Here $\rho_1 = \rho + \frac{1}{2}\Delta\rho$, $\rho_2 = \rho + \frac{3}{2}\Delta\rho$, etc. (c) A control volume between the ρ and $\rho + \Delta\rho$ isopycnals and their surface extensions, showing the diffusive and surface fluxes into and out of it.

Note that this relation for water mass formation holds for both steady and time-varying cases.

3) THE ''EXTENDED ISOPYCNAL'' AND THE ''NET'' DIFFUSIVE DENSITY FLUX

It is useful to generalize the diapycnal density flux D so as to include the surface density flux. We thus define the ''surface extension'' of the isopycnal to lie along the ocean surface where the isopycnal is too light to exist—this ''surface extension'' is denoted by the dashed line in the schematic Fig. 3a. The total flux across this surface extension

$$D_{\rm surf}(\rho) = \int_{\{\mathbf{x}:\rho<\rho_m(\mathbf{x})\}} \mathcal{D}_{\rm in}\, dA \tag{8}$$

(here ρ_m is the mixed layer density) is equal (see Fig. 3b) to the density influx into the outcrops of all the water denser than ρ,

$$D_{\rm surf}(\rho) = \int_{\rho_m>\rho} F(\rho_m)\, d\rho_m. \tag{9}$$

Hence

$$-\frac{\partial D_{\rm surf}}{\partial \rho} = F, \tag{10}$$

and combining (7) and (10) gives

$$G(\rho) = -\frac{\partial D_{\rm diff}}{\partial \rho} - \frac{\partial D_{\rm surf}}{\partial \rho} \equiv -\frac{\partial D_{\rm net}}{\partial \rho}, \tag{11}$$

where

$$D_{\rm net} = D_{\rm surf} + D_{\rm diff} \tag{12}$$

is the total nonadvective diapycnal density flux across the extended isopycnal made up of the isopycnal and its surface extension, that is, the flux into the waters denser than ρ.

Equation (11) then states that the diapycnal volume flux is given by the convergence of the net diapycnal density flux, $-\partial D_{\rm net}/\partial\rho$, into the control volume made up of the region between the two isopycnals and their surface extensions (Fig. 3c).

Accordingly, the water mass formation, M, is related to the net diapycnal density flux across the extended isopycnal by

$$M = \frac{\partial^2 D_{\rm net}}{\partial \rho^2}. \tag{13}$$

b. Idealized example 1: Water mass formation by surface fluxes alone

As an illustration of Walin's formulation, consider an idealized example where a basin gains density everywhere at the surface ($F > 0$) and there is no mixing; that is, $D_{\rm net} = D_{\rm surf}$. Suppose $\rho_{\rm dense}$ is the density of the densest isopycnal that outcrops and that the lightest water that exists anywhere in the basin has density $\rho_{\rm min}$ (see Fig. 4a). The surface density gain leads to $D_{\rm surf}$ being positive over all the isopycnals that outcrop ($\rho_{\rm dense} > \rho > \rho_{\rm min}$); but it is zero for denser isopycnals with $\rho > \rho_{\rm dense}$ (shaded in Fig. 4a) that are unventilated within the domain. A hypothetical form for $D_{\rm surf}$ in this cooling case is shown in Fig. 4b. Note that $D_{\rm surf}(\rho_{\rm min})$ is the same as the total density gain over the basin since the area $\rho_m(\mathbf{x}) > \rho_{\rm min}$ in (8) covers the whole surface of the basin.

In this example, since there is density gain everywhere, $\partial D_{\rm surf}/\partial\rho = -F$ is (Fig. 4c) always negative [see (8) and (10)], and the maximum value of $D_{\rm surf}$ is attained (Fig. 4b) for the lightest water at $\rho_{\rm min}$.

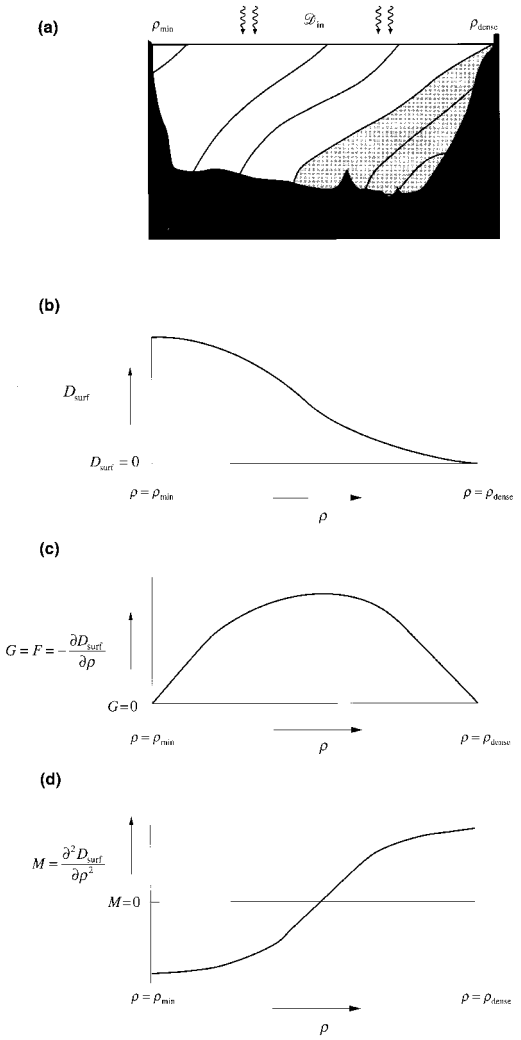

FIG. 4. (a) Schematic section through an idealized basin with surface density gain and no mixing. The lightest water in the basin has density ρ_{min} and ρ_{dense} is the densest water that outcrops; water denser than ρ_{dense} is shaded. (b) The variation of the surface-integrated density flux $D_{surf}(\rho)$ with ρ, (c) the implied diapycnal volume flux $G(\rho) = F = -\partial D_{surf}/\partial\rho$, and (d) the water mass formation rate $M(\rho) = -\partial G/\partial\rho$. In this example, the surface density input drives a diapycnal volume flux toward denser waters in (c), which leads to the densest waters being formed at the expense of the lightest waters in (d).

The surface density gain (11) drives a diapycnal volume flux (Speer and Tziperman 1992):

$$G(\rho) = F = -\frac{\partial D_{surf}}{\partial \rho}. \tag{14}$$

Since there is surface density influx, $F > 0$ (or alternatively a convergence in D_{surf}), the diapycnal volume flux $G(\rho)$ is directed (Fig. 4c) from light to dense water.

The resulting water mass formation $M(\rho)$ is a consequence of the convergence of the diapycnal volume flux,

$$M(\rho) = -\frac{\partial G}{\partial \rho}.$$

As the surface forcing induces $G(\rho) > 0$ within the domain and by definition $G(\rho) = 0$ for isopycnals outside the physical domain, then there is a convergence of G (hence positive M) at high ρ and a divergence of G (hence negative M) at low ρ (Figs. 4c, d). Therefore, the surface forcing drives a formation of dense water and a compensating destruction of light water.

This formation of dense water either leads to the basin filling up with denser water or the export of dense water from the basin through an open boundary. Thus, in this example, a steady-state solution over a closed domain cannot be achieved.

c. Idealized example 2: The steady state in a closed basin

In a steady state in a closed basin, there is no water mass formation at any density, so $M \equiv G \equiv D_{net} \equiv 0$. The total density flux $D_{net}(\rho) = D_{surf}(\rho) + D_{diff}(\rho)$ must be zero down into the region (shaded in Fig. 5a) below any extended isopycnal; that is, the region occupied by water denser than ρ. Otherwise the density content of this region would change. In the artificial limit of no diffusion, the surface forcing would have to adjust such that $D_{surf}(\rho) \equiv 0$. However, diffusion always mixes fluid, so giving $-$ve D_{diff} (arrow going from dense water to light in Fig. 5a; the dashed line in Fig. 5b). Hence with diffusion a steady state with $D_{net} \equiv 0$ implies that the surface densities (or fluxes) must adjust so that $D_{surf} > 0$ (dotted line in Fig. 5b) for all ρ: the surface fluxes must act so as to *increase* the density contrast.

Note that the diffusive flux must disappear ($D_{diff} = 0$) across the isopycnal surfaces for the lightest $\rho = \rho_{min}$ and heaviest $\rho = \rho_{max}$ waters, as the area of these isopycnal surfaces falls to zero. Here D_{diff} reaches a maximum magnitude for some intermediate density with a large isopycnal area. The gradient of D_{diff} is negative for low ρ and positive for high ρ, so it makes (Fig. 5c) low ρ waters denser ($G_{diff}(\rho) > 0$) and high ρ waters lighter ($G_{diff}(\rho) < 0$). Conversely the surface fluxes F attempt to make light waters lighter and dense waters denser (Figs. 5a, c).

3. Mixing processes

We wish to separate the interior diffusive flux, D_{diff}, into separate contributions within the mixed layer, at its base, and within the thermocline proper. Accordingly, we split up the isopycnal into different parts as shown in Fig. 6:

- ***a*** marks the short vertical segments where the isopycnal outcrops within the mixed layer. Lateral mixing within the mixed layer across these outcrops drives a component of diffusive flux across the isopycnal. This lateral density flux is denoted as D_{lat}.

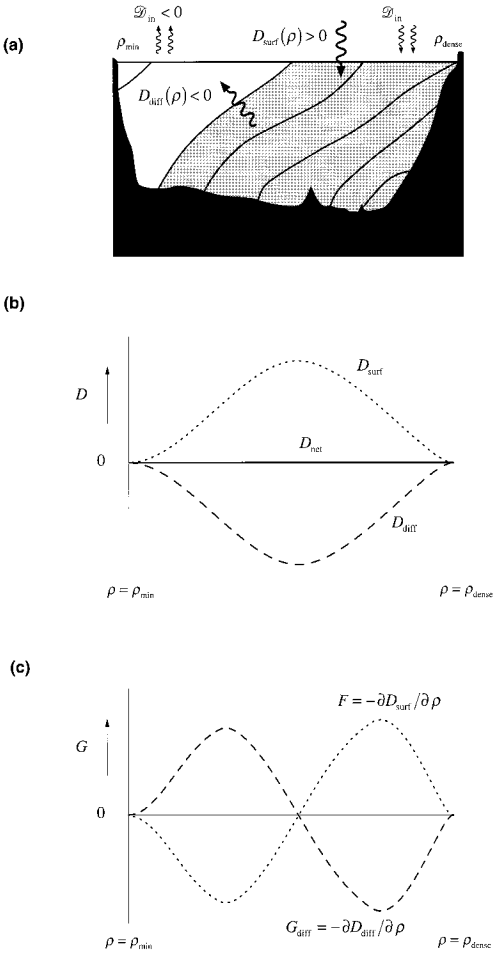

FIG. 5. (a) Schematic section through an idealized basin in steady state, with zero net surface density gain and mixing. As in Fig. 4, ρ_{min} and ρ_{dense} are the lightest and densest outcropping waters. Water denser than an arbitrary density ρ is now shaded. (b) The variation of the surface-integrated density flux $D_{surf}(\rho)$ (dotted line), the diffusive flux $D_{diff}(\rho)$ (dashed line), and the net flux $D_{net}(\rho)$ with ρ. (c) The surface density input into isopycnal layers $F(\rho) = -\partial D_{surf}/\partial\rho$ and the diffusive density input into isopycnal layers $G_{diff}(\rho) = -\partial D_{diff}/\partial\rho$.

- ***b*** marks the near-horizontal segments where the isopycnal lies within the ''bundle'' of isopycnals within the strong density gradient at the base of the mixed layer. The density flux through this part of the isopycnal is denoted as D_{ent}.
- ***c*** denotes the isopycnal within the thermocline proper. The diffusive density flux within the thermocline is denoted as D_{thermo}.

Thus, the interior diffusive density flux through the isopycnal is given by

$$D_{diff} = D_{lat} + D_{ent} + D_{thermo}. \tag{15}$$

We now discuss these various mixing processes, performing a scale analysis to estimate their relative importance.

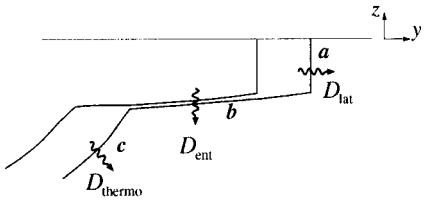

FIG. 6. The diffusive diapycnal flux D_{diff} acting in the interior of the ocean is split into components due to (a) lateral mixing in the mixed layer D_{lat}, (b) entrainment mixing at the base of the mixed layer D_{ent}, and (c) mixing within the thermocline proper D_{thermo}.

a. Lateral mixing within the mixed layer

Lateral mixing within the mixed layer is driven by eddies in baroclinically unstable regions. The horizontal density flux per unit area **D** is often parameterized by

$$\mathbf{D} = -\kappa_h \nabla\rho_m,$$

with κ_h the horizontal (eddy) diffusivity. The total lateral flux across the ρ isopycnal is then given (here h is the depth of the mixed layer) by

$$D_{lat}(\rho) = -\int_{\rho_m(\mathbf{x})=\rho} h\kappa_h|\nabla\rho_m|\, dl \approx L_{EW}\cdot h\cdot\kappa_h\overline{|\nabla\rho_m|}, \tag{16}$$

assuming that the isopycnals are aligned roughly east–west and writing L_{EW} as the zonal width of the basin. The overbar denotes an average taken along the outcrop. This mixing is most likely to be important where the mixed layer is both deep and has strong lateral gradients, as in the winter North Atlantic near the Gulf Stream and Labrador Current (see, e.g., Fig. 13 and the model diagnosis of Marshall et al. 1998).

In such regions the annual-average (denoted by the angle brackets) lateral flux $\langle D_{lat}\rangle$ will be about half its winter value, as the winter mixed layer depth $h_{winter} >$ 200 m is much greater than the summer depth $h_{summer} \sim$ 20 m:

$$\langle D_{lat}(\rho)\rangle \sim \frac{1}{2}L_{EW}\cdot h_{winter}\cdot\kappa_h\overline{|\nabla\rho_m|}. \tag{17}$$

Moreover the mean density gradient $\overline{|\nabla\rho_m|}$ will be dominated by its value in regions where it becomes large, such as western boundary currents (WBCs). Suppose that the isopycnal runs along a WBC for $\sim 10^3$ km, the diffusivity $\kappa_h \sim 1000$ m^2 s^{-1} (see, e.g., Haine and Marshall 1998), the density gradient is 10^{-5} kg m^{-4} (1 kg m^{-3} in $\sim$100 km) and the winter mixed layer depth reaches 400 m. Then $\langle D_{lat}\rangle \sim 2\times 10^6$ kg s^{-1}.

b. Mixing at the base of the mixed layer

There is enhanced mixing near the base of the surface mixed layer through the action of the wind, penetrative convection, and internal wave breaking, which is parameterized in mixed layer models (see Large et al. 1994

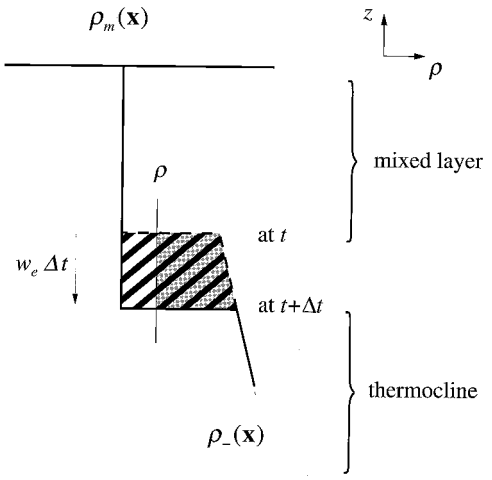

FIG. 7. Schematic of diapycnal flux due to entrainment. In a time Δt, a thickness $w_e\Delta t$ of thermocline fluid is entrained into the mixed layer. In doing so, the fluid decreases its density from ρ_- to ρ_m, and density content $w_e\Delta t(\rho_- - \rho_m)$ per unit area (the hashed region) is removed from the entrained water and mixed up into the mixed layer. The density content contained in fluid denser than ρ, for $\rho_m < \rho < \rho_-$, is reduced by $w_e\Delta t(\rho_- - \rho)$, the shaded area.

for a review). In particular, mixing occurs whenever dense thermocline water is entrained into the lighter mixed layer.

1) THE ENTRAINMENT FLUX PER UNIT AREA, $\mathcal{D}_{\text{ent}}$

We now evaluate the entrainment flux across isopycnals lying at the base of the mixed layer. The rate of entrainment of fluid into the mixed layer

$$w_e = w_b + \frac{\partial h}{\partial t} + \mathbf{u}_b \cdot \nabla h, \tag{18}$$

where w_b and $\mathbf{u}_b$ are the vertical and horizontal velocities at the base of the mixed layer. Entrainment can result from either (i) sustained upwelling in equatorial and eastern boundary regions ($w_b > 0$), (ii) the seasonal deepening of the mixed layer in autumn and winter ($\partial h/\partial t > 0$), or (iii) net annual heat loss, giving a winter mixed layer deepening from year to year ($\mathbf{u}_b \cdot \nabla h > 0$), as happens as fluid moves northward in the western and northern North Atlantic. However, the density differences at the base of the winter mixed layer are too small for the entrainment driven by winter-on-winter deepening (iii) to be significant in mixing density.

As thermocline water is entrained into the mixed layer, the water crosses the strong density gradient at the base of the mixed layer (Fig. 7). There is a density jump $\Delta\rho = \rho_- - \rho_m$, from its thermocline value $\rho_-(\mathbf{x})$ to its value in the mixed layer $\rho_m(\mathbf{x})$.

Over a time Δt, a thickness $w_e\Delta t$ of thermocline water has its density decreased by $\Delta\rho$ from ρ_- to ρ_m. Hence density content $w_e\Delta t\Delta\rho$ per unit area (the hashed region in Fig. 7) is removed from the entrained water and mixed up into the rest of the mixed layer. In other words, there is a density flux per unit area $w_e\Delta\rho = w_e(\rho_- - \rho_m)$ up into the mixed layer and across the ρ_m isopycnal.

However, we wish to find the density flux across a general ρ surface lying within the density jump, $\rho_m < \rho < \rho_-$. As water is entrained up into the mixed layer, the density content of the isopycnals denser than ρ decreases by $w_e\Delta t[\rho_-(\mathbf{x}) - \rho]$ per unit area (shaded in Fig. 7). Hence the instantaneous entrainment density flux per unit area $\mathcal{D}_{\text{ent}}(\rho, \mathbf{x})$ *down* across the ρ isopycnal is

$$\mathcal{D}_{\text{ent}}(\rho, \mathbf{x}) = -w_e(\mathbf{x})(\rho_-(\mathbf{x}) - \rho). \tag{19}$$

In reality, of course, the density jump is smoothed into a transition zone of strong but finite density gradient. An advection/diffusion transition layer of thickness κ_v/w_e forms, where κ_v is the vertical diffusivity. However, as long as the scale of variation of w is greater than the transition layer thickness so that fluid passes through all the isopycnals at a rate w_e, (19) still holds.

Values of diffusivity immediately below the mixed layer vary widely. The strong shear in equatorial upwelling zones gives comparatively large diffusivities, and hence thick transition layers, ~50 m deep (Peters et al. 1988), a scale similar to that over which the vertical velocity w varies (Bryden and Brady 1985). Here, therefore, (19) will not hold, so the mixing driven by equatorial upwelling is best considered as a thermocline diffusion. In midlatitudes the shears and hence the diffusivity are weaker, and the density gradient is much sharper (see, e.g., Brainerd and Gregg 1996). The transition layer is thus typically much thinner than the scale over which w varies, so the mixing driven by the seasonal mixed layer cycle at midlatitudes can be thought of as an entrainment flux.

We thus focus on the process of seasonal entrainment and now estimate its basin-integrated importance.

2) THE BASIN-INTEGRATED SEASONAL ENTRAINMENT FLUX

Integrating (19) over the whole basin gives the basin-integrated entrainment flux

$$D_{\text{ent}}(\rho) = -\int_{\mathcal{A}_{\text{base}}} w_e[\rho_-(\mathbf{x}) - \rho]\, dA. \tag{20}$$

Here $\mathcal{A}_{\text{base}} = \{\mathbf{x} : \rho_m(\mathbf{x}) < \rho < \rho_-(\mathbf{x})\}$ is the area where the ρ isopycnal lies within the base of the mixed layer (Fig. 8).

Along the northern boundary of the region $\mathcal{A}_{\text{base}}$, the isopycnal outcrops (Fig. 8) into the mixed layer, $\rho = \rho_m$, and $\rho_- - \rho = \Delta\rho$ (which will, in general, vary along this outcrop). Moving south through $\mathcal{A}_{\text{base}}$, $\rho_- - \rho$ declines until at its southern end the isopycnal passes into the thermocline and $\rho_- - \rho$ falls to zero. Hence the basin-integrated entrainment flux across the ρ isopycnal might be

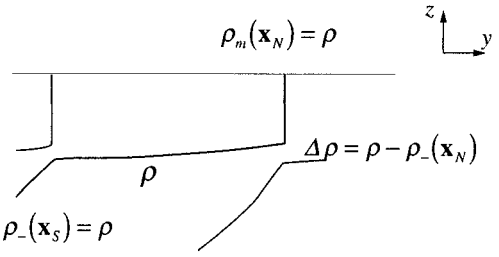

FIG. 8. Idealized schematic through the region $\mathcal{A}_{\text{base}}$ where the ρ isopycnal runs along the base of the mixed layer. Along the northern boundary of the region $\mathbf{x} = \mathbf{x}_N$, the isopycnal outcrops into the mixed layer $\rho = \rho_m(\mathbf{x}_N)$ and $\rho_- - \rho = \Delta\rho(\mathbf{x}_N)$. Moving south through $\mathcal{A}_{\text{base}}$, $\rho_- - \rho$ declines until along its southern boundary $\mathbf{x} = \mathbf{x}_S$ the isopycnal passes into the thermocline $\rho = \rho_-(\mathbf{x}_S)$.

$$D_{\text{ent}} \approx \frac{1}{2} w_e \overline{\Delta\rho} \cdot \mathcal{A}_{\text{base}}, \tag{21}$$

where the overline denotes the along-outcrop mean of $\Delta\rho$.

We now need to estimate the area $\mathcal{A}_{\text{base}}(\rho)$. The zonal-mean meridional extent of $\mathcal{A}_{\text{base}}(\rho)$ is

$$L_{\text{base}} \sim \overline{\Delta\rho \Big/ \frac{\partial\rho_-}{\partial y}}, \tag{22}$$

where $\partial\rho_-/\partial y$ is the gradient of the ''top of thermocline'' density ρ_-. Like the entrainment flux, L_{base} is proportional to the density jump $\Delta\rho$. The area $\mathcal{A}_{\text{base}}(\rho)$ is then $\sim L_{\text{base}} L_{\text{EW}}$, where L_{EW} is the zonal width of the basin.

Hence the basin-integrated contribution to the entrainment flux

$$D_{\text{ent}} \sim \frac{1}{2} w_e \Delta\rho \cdot \mathcal{A}_{\text{base}} \sim \frac{1}{2} w_e \overline{(\Delta\rho)^2 \left(\frac{\partial\rho}{\partial y}\right)^{-1}} \cdot L_{\text{EW}}, \tag{23}$$

where again the overbar denotes the outcrop-mean.

Note that, since both the area-averaged entrainment flux, (21), and the area over which it exists (22) are proportional to the density jump $\Delta\rho$, the *integrated* flux D_{ent} is proportional to $(\Delta\rho)^2$.[1]

In spring and early summer the mixed layer retreats and there is no density jump at its base, so $\Delta\rho \approx 0$; while from late summer to mid winter, $\Delta\rho \approx 1.0$–0.4 kg m^{-3}. See the temperature profiles at OWS Papa (Fig. 1), where ΔT ranges from 4° to 2°C from July to November. Hence, the entrainment flux is only significant from late summer to early winter—''autumn.'' Where the mixed layer becomes deeper than 80–100 m, the density jump generally becomes insignificant. We therefore introduce the notation

$$[h] = h_{\text{early winter}} - h_{\text{summer}} \tag{24}$$

for the change (~50–100 m) in mixed layer depth over the autumn period while there is still a substantial density jump at its base.

Using (24) we can integrate (23) over the year, assuming that the entrainment rate $w_e \approx \partial h/\partial t$, which gives an estimate for the annual-mean entrainment mixing driven by the seasonal cycling as

$$\langle D_{\text{ent}} \rangle \sim \frac{1}{2} \tau_{\text{year}}^{-1} [h] \overline{(\Delta\rho)^2 \left(\frac{\partial\rho}{\partial y}\right)^{-1}} \cdot L_{\text{EW}}, \tag{25}$$

where $(\Delta\rho)^2$ is the entrainment-weighted mean over the autumn period and τ_{year} the length of a year.

A plausible density gradient in the midlatitudes is ~6 × 10^{-7} kg m^{-4} (1.2 kg m^{-3} in 20° of latitude). From the OWS Papa data, a typical autumn value of the density jump $\Delta\rho$ might be ≈0.8 kg m^{-3}, and the autumn mixed layer change $[h]$ might be ~80 m. Choosing a basin width appropriate to the Atlantic, L_{EW} ~4 × 10^6 m then gives $\langle \mathcal{D}_{\text{ent}}(\rho) \rangle$ ~5 × 10^6 kg s^{-1}. Assuming $c_p\rho = 4 \times 10^6$, $d\rho/dT = 0.25$ kg m^{-3} °C^{-1}, this density flux is equivalent to a heat flux of ~0.1 PW across the isopycnal.

Now the diapycnal *volume* flux across the isopycnal driven by this entrainment mixing $G_{\text{ent}} = -\partial D_{\text{ent}}/\partial\rho$. Assume that the annual average $\langle D_{\text{ent}} \rangle$ of 6 × 10^6 kg s^{-1} is achieved in the North Atlantic at $\sigma \approx 26.0$ and that the outcrops become very small in area by $\sigma \approx 28.0$ so that $\langle D_{\text{ent}} \rangle$ disappears at $\sigma \approx 28.0$. Then a mean value of G_{ent} over these densities is $\Delta\langle D_{\text{ent}} \rangle/\Delta\rho \approx 3$ Sv (Sv ≡ 10^6 m^3 s^{-1}), consistent with the estimate of Garrett and Tandon (1997).

c. Diapycnal mixing in the thermocline

The basin-integrated interior diffusive density flux $D_{\text{thermo}}(\rho)$ is defined as

$$D_{\text{thermo}}(\rho) = \int_{\{\mathbf{x}:\rho_{\text{bot}}(\mathbf{x}) > \rho > \rho_m(\mathbf{x})\}} \kappa_d \partial\rho/\partial z \, dA, \tag{26}$$

where $\rho_{\text{bot}}(\mathbf{x})$ is bottom density and $\partial\rho/\partial z$ is the local vertical gradient of ρ. This flux, however, is difficult to scale, given the variability in vertical diffusivity (see Caldwell and Moum 1995 for a review) and stratification. Recent tracer release experiments have emphasized that the vertical diffusivity in the interior of the ocean is only of the order 10^{-5} m^2 s^{-1} (Ledwell et al. 1993). In contrast, the mixing may be greatly enhanced near the boundaries, such as near sidewalls (Armi 1978; Toole et al. 1994) and near the seafloor (Polzin et al. 1995).

d. Comparison of mixing processes

In the steady state over a closed basin, as in the example discussed in section 2c, the total density flux down into waters deeper than ρ,

$$D_{\text{net}} = D_{\text{surf}} + D_{\text{ent}} + D_{\text{lat}} + D_{\text{thermo}} \equiv 0.$$

[1] Garrett and Tandon's (1997) expression for the diapycnal *volume* flux G_{ent} may be recovered by differentiating (23) by ρ.

Since it is difficult to scale $D_{\text{thermo}}(\rho)$, we shall instead scale D_{lat} and the seasonal component of D_{ent} against D_{surf}, the flux across the ocean surface into waters denser than ρ. Now the annual mean

$$\langle D_{\text{surf}}(\rho)\rangle = \left\langle \int_{\{\mathbf{x}:\rho<\rho_m(\mathbf{x})\}} \mathcal{D}_{\text{in}}\, dA \right\rangle \sim \overline{\mathcal{D}_{\text{in}}} \cdot L_{\text{EW}} \cdot L_{\text{NS}},$$

where $\overline{\mathcal{D}_{\text{in}}}$ is the annual-mean area-mean density gain north of the outcrop and, again, L_{EW} and L_{NS} are estimates of the zonal and meridional scale of the region poleward of the ρ outcrop.

Assuming $\overline{\mathcal{D}_{\text{in}}} \sim 2 \times 10^{-6}$ kg m^{-2} s^{-1} (equivalent to a heat loss of $\sim$40 W m^{-2}) over this region north of the isopycnal outcrop, together with $L_{\text{EW}} \sim 4 \times 10^6$ m, $L_{\text{NS}} \sim 3 \times 10^6$ m implies a $\langle D_{\text{surf}}(\rho)\rangle \sim 24 \times 10^6$ kg s^{-1}. This estimate is consistent with climatological values for the North Atlantic [see, e.g., that derived from the climatology of Esbensen and Kushnir (1981), the dotted line in Fig. 11] and is clearly considerably larger than the values (2–5 $\times 10^6$ kg s^{-1}) estimated in sections 3a and 3b for the lateral mixing and seasonal entrainment terms. In the steady state, this *surface flux* must largely be balanced by thermocline diffusion over a closed basin or possibly result in water mass transformation over an open domain.

The surface flux dominates, for example, the seasonal entrainment flux for two main reasons: (i) the magnitude of the annual-mean surface flux north of the outcrop $\overline{\mathcal{D}_{\text{in}}}$, is greater than the entrainment flux $\mathcal{D}_{\text{ent}}$ and (ii) the north–south extent of the region poleward of the outcrop, L_{NS}, is much greater then the north–south extent of the entrainment region, L_{base}.

We now estimate the relative importance of the two mixed layer contributions: the lateral diffusive flux and the seasonal entrainment flux. From (25) and (17)

$$\frac{\langle D_{\text{lat}}(\rho)\rangle}{\langle D_{\text{ent}}(\rho)\rangle} \sim \frac{\kappa_h \overline{|\nabla \rho_m|}}{\tau_{\text{year}}^{-1}(\Delta\rho)^2 \overline{\left(\frac{\partial\rho}{\partial y}\right)^{-1}}} \cdot \frac{h_{\text{winter}}}{[h]}, \qquad (27)$$

where the overbars denote the average along the outcrop and we have assumed that h_{winter} and $[h]$ vary relatively little along the outcrop.

Hence, $\langle D_{\text{lat}}(\rho)\rangle$ will be relatively more important than $\langle D_{\text{ent}}(\rho)\rangle$ for (a) $h_{\text{winter}} \gg [h]$, that is, winter mixed layers much deeper than $\sim$100 m; (b) large diffusivity κ_h; (c) large $\overline{|\nabla\rho_m|}$; (d) small $\Delta\rho$ in autumn; and (e) large $\overline{(\partial\rho/\partial y)^{-1}}$, giving a small entrainment region width

$$L_{\text{base}} \sim \Delta\rho \Big/ \overline{\frac{\partial\rho}{\partial y}}.$$

Hence for denser isopycnals, outcropping in the subpolar gyre where winter mixed layers are deep, lateral diffusion is more important, while for midlatitude isopycnals outcropping into shallower mixed layers seasonal entrainment is more significant, especially where there is a large density jump at the base of the mixed layer.

It is important to note that a large outcrop-averaged mixed layer density gradient can be consistent with a relatively wide entrainment region. The outcrop-averaged mixed layer density gradient is much greater than the reciprocal of the outcrop-averaged mean isopycnal spacing $\overline{|\nabla\rho_m|} \gg [\overline{(\partial\rho/\partial y)^{-1}}]^{-1}$ if the isopycnal separation varies strongly across the basin, as it will do if the isopycnals lie close together within a western boundary current and then spread out in the ocean interior.

In the following section, we assess the importance of each of these diffusive terms in a general circulation model of the North Atlantic.

4. Diagnosing water mass formation

a. The ocean model

In the present study, we examine the formation of water masses in a coupled mixed layer and isopycnic model of the North Atlantic. We employ a 30-yr run of the Miami Isopycnic Model (MICOM), developed by Bleck and his coworkers (Bleck et al. 1989; Bleck et al. 1992). The forcing and model configuration are as discussed in New et al. (1995).

A Kraus–Turner mixed layer overlies 19 isopycnic layers representing the ocean interior with potential density anomaly $\sigma \equiv \rho_{\text{pot}} - 1000$ kg m^{-3} ranging from 25.65 to 28.15. Here ρ_{pot} is potential density referenced to atmospheric pressure; in the following it is simply written ρ. The model is run over a (closed) domain (approximately from 15°S to 82°N over the North Atlantic). The model grid is based on a rotated Mercator projection, with a horizontal resolution of around 1°.

The model employed here (v2.4) includes diapycnic diffusion. The diapycnic diffusivity κ_d is parameterized (Hu 1996) as

$$\kappa_d = c/N, \qquad (28)$$

where we take $c = 10^{-7}$ m^2 s^{-2}, and $N = (-g\rho^{-1}\partial\rho/\partial z)^{1/2}$ is the buoyancy frequency. This yields typical values of κ_d of 1×10^{-5} m^2 s^{-1} in the thermocline and 1×10^{-4} m^2 s^{-1} in the deep ocean.

The model is initialized from the September values of the Levitus (1982) dataset and integrated for 30 years. It is forced by a wind stress from the monthly mean climatology of Hellerman and Rosenstein (1983). The surface heat and freshwater fluxes are evaluated from the sum of climatological heat and freshwater fluxes [from Esbensen and Kushnir (1981) and Jaeger (1976)] and a linear relaxation of surface temperature and salinity to monthly mean and interpolated seasonal climatology from Levitus (1982) to avoid an unrealistic model drift (following Haney 1971). Thus, the surface heat flux out of the ocean, $\mathcal{H}_{\text{out}}$, is given by

$$\mathcal{H}_{\text{out}} = \mathcal{H}_{\text{cli}} - \lambda(T - T_{\text{Lev}}), \qquad (29)$$

where $\mathcal{H}_{\text{cli}}$ is the climatological heat flux, T and T_{Lev} are

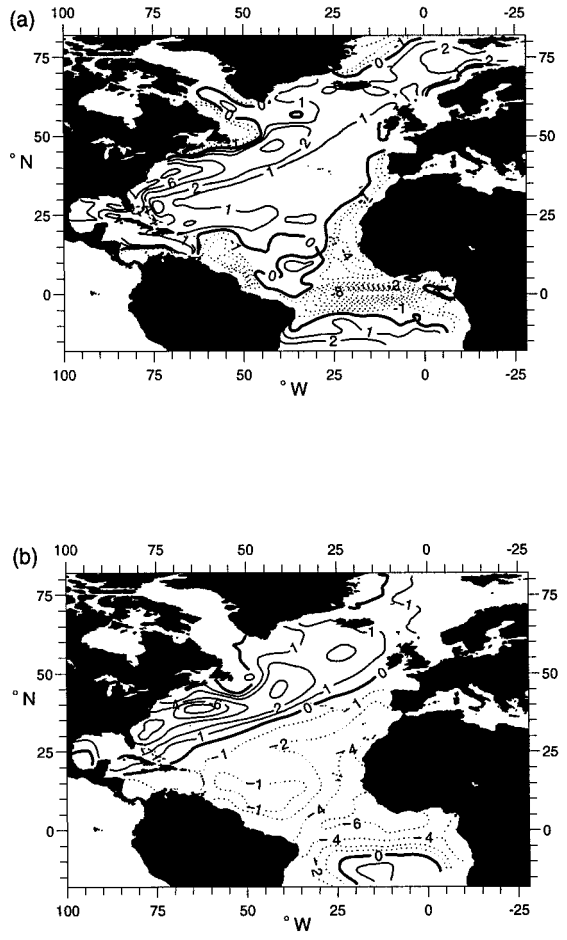

FIG. 9. (a) The annual-average field of surface density flux $\langle \mathcal{D}_{\text{in}} \rangle$ (10^{-6} kg m^{-2} s^{-1}) applied over the model domain and (b) the annual surface density flux from the climatological fluxes. The difference in the two fields is due to the Haney relaxation term being included in the model forcing, which acts to reduce the density loss in the Tropics implied from the climatological fluxes. Positive values represent a flux of density into the ocean.

the surface temperature in the model and Levitus climatology, and the relaxation coefficient $\lambda = 35$ W m^{-2} K^{-1}. This Haney relaxation is found to substantially modify the climatological forcing.

b. Surface and diffusive integrated density fluxes

1) SURFACE FORCING

We are interested in the net-annual water mass production. Hence we consider *annual-averaged* fluxes, evaluated by ''online'' integration over model year 31.

The annual-averaged surface density flux applied in the model is shown in Fig. 9a. Assuming an expansion coefficient $\alpha_E = -\rho^{-1} d\rho/dT = 2.5 \times 10^{-4}$ K^{-1}, a density influx of 10^{-6} kg s^{-1} m^{-2} is equivalent to a heat outflux of $\sim$17 W m^{-2}. As expected, there is a net gain of density generally north of a zero line running from 10°N, 60°W to 45°N, 10°W and a loss south of it. This surface flux is the sum of the climatological fluxes and the relaxation (29). In comparison, the climatological density flux shown in Fig. 9b shows a greater density loss in the Tropics and has a zero line that lies farther north.

In applying Walin's relations, however, we need to calculate annual averages following isopycnals as they move from season to season. The annual-averaged diapycnal surface flux $\langle D_{\text{surf}}(\rho) \rangle$ across the surface extension of the ρ isopycnal is then given, writing τ_{year} as the length of the year, by

$$\langle D_{\text{surf}}(\rho) \rangle = \frac{1}{\tau_{\text{year}}} \int_{\text{year}} \int_{\{\mathbf{x}:\rho_m(\mathbf{x})>\rho\}} \mathcal{D}_{\text{in}} \, dA \, dt. \quad (30)$$

The finite-difference forms for $\langle D_{\text{surf}}(\rho) \rangle$ and other diagnosed fluxes are shown in the appendix. For clarity, in the following, we shall drop the explicit notation $\langle \, \rangle$ for the annual mean, and D, G, and M should be read as annual means.

The surface flux D_{surf} (the dotted line in Fig. 10a) is positive over all the outcropping layers in the domain $\sigma_{\text{min}} \approx 20.0 < \rho < \sigma_{\text{dense}} \approx 28.15$ and is zero for any denser, unventilated layers $\sigma > \sigma_{\text{dense}}$ (like those shaded in the schematic Fig. 4a). Here D_{surf} is positive for the lightest water $\sigma = \sigma_{\text{min}} \approx 20.0$ since there is a slight basin-integrated density gain by the model (average value $\sim 6 \times 10^{-8}$ kg s^{-1} m^{-2} $\sim$ a heat loss of 1.3 W m^{-2}). Note that waters lighter than $\sigma = 25.65$ (denoted by the vertical gray line in Fig. 10 and succeeding figures) only exist within the mixed layer.

Given that $D_{\text{surf}}(\rho)$ is the surface density input into all the isopycnals with density greater than ρ (9),

$$D_{\text{surf}}(\rho) = \int_{\rho'>\rho} F(\rho') \, d\rho',$$

it follows that the negative of the slope of D_{surf} gives F, the surface density input into an isopycnal range per unit of density (the dotted line in Fig. 10b). Denser isopycnals ($\sigma > 25.4$) outcrop into the mixed layer to the north and so receive annual-averaged density gain, while the lighter isopycnals $\sigma < 25.4$ outcrop in the Tropics and so lose density. Hence D_{surf} peaks at $\sigma = 25.4$, and the slope of D_{surf} changes from positive for $\sigma < 25.4$ to negative for $\sigma > 25.4$. This lightening of light waters and making dense of dense waters means that the surface forcing acts to *increase* the density contrast across the basin, as in the idealized example of the steady state in section 2c.

The density flux $D_{\text{surf}}(\rho)$ (30) is the sum of the climatological forcing and a Haney-style relaxation (29). The climatological component is denoted by the dotted line in Fig. 11. It is large and negative for $\sigma = \sigma_{\text{min}} \approx 20.0$ because the Esbensen and Kushnir climatology gives a basin-integrated density loss over the North Atlantic. This density loss is concentrated over the Tropics (Fig. 9b); hence the steep positive slope of the dashed

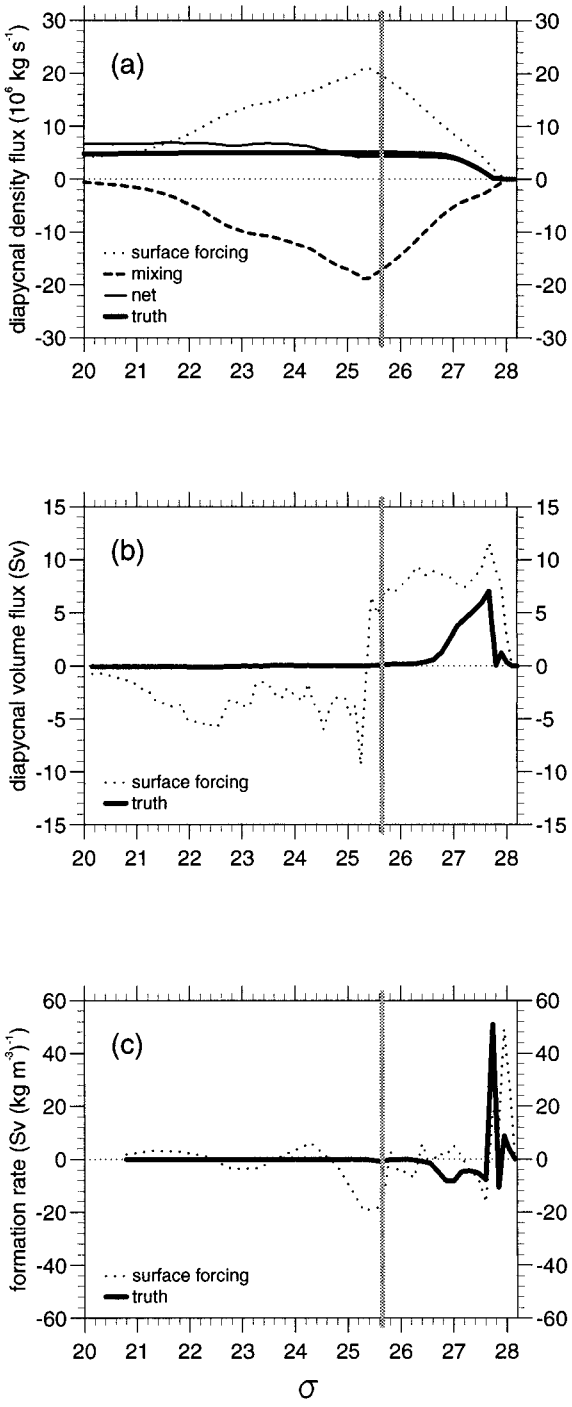

FIG. 10. Annual-mean water mass diagnostics evaluated over the whole basin for (a) the diffusive density flux $D(\rho)$ (10^6 kg s^{-1}), (b) the diapycnal volume flux $G(\rho)$ (Sv), and (c) the water mass formation rate $M(\rho) = -\partial G/\partial\rho$, (Sv/kg m^{-3}) all over the range $20 < \rho < 28$. For the density flux, the surface contribution D_{surf} is denoted by a thin dotted line, the mixing by a dashed line, the net contribution D_{net} from the sum of the surface forcing and mixing by a thin full line, and that consistent with the model truth by the thick solidline. In the plots of the diapycnal volume flux and formation rates, independent model truth is denoted by a thick full line. The gray bar at $\sigma = 25.65$ denotes the density of the lightest thermocline waters resolved by the model.

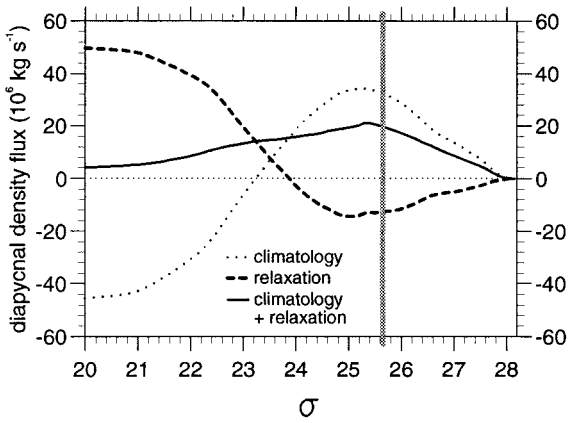

FIG. 11. Annual-mean surface density flux integrated over the whole basin $D_{\text{surf}}(\rho)$ is shown by the full line. The separate contributions from the climatological forcing and the Haney-style relaxation are shown by the dotted and dashed lines, respectively. Units are 10^6 kg s^{-1}.

line in Fig. 11 over the lighter densities. The implied net lightening is contrary to the normal view of the North Atlantic as exporting cold, dense water and importing warm, light water. The Haney forcing (the dashed line in Fig. 11) opposes this excessive density loss over the Tropics, giving a much more realistic net basin-integrated density gain (solid line).

The climatological forcing also has a larger maximum at $\sigma = 25.4$ than the total surface flux; here the Haney relaxation is acting to weaken the ''unmixing'' driven by the surface forcing.

Different climatologies, of course, will give different F and D_{surf}. Speer and Tziperman (1992) used surface fluxes from the climatology of Isemer and Hasse (1987) and found F reaching a maximum of 30 Sv at $\sigma = 26.3$ (their Fig. 6b). However, the climatology of Esbensen and Kushnir (1981) used in our model gives (not shown) a maximum diapycnal volume flux of only 19 Sv, at $\sigma = 26.5$, which is reduced further (dotted line in Fig. 10b) to 12 Sv (both in the full domain and in that part of the domain north of 24°N) by including the Haney relaxation term.

2) DIFFUSIVE INTERIOR FLUXES AND THE BALANCE WITH SURFACE FLUXES

The density flux across the ρ isopycnal from interior mixing, D_{diff}, is plotted as the dashed line in Fig. 10a. The diffusive density flux D_{diff} transfers density from dense to light waters and so is *negative* with the sign convention we employ here. It acts to *reduce* the density contrast across the basin and hence oppose the action of the surface forcing.

The sum $D_{\text{net}} = D_{\text{surf}} + D_{\text{diff}}$ (the thin full line in Fig. 10a) is the total density flux downward across the extended isopycnal (Fig. 3b) into the region of fluid whose density is greater than ρ. In a closed basin in a steady

state (section 3) $D_{net}(\rho)$ would be zero for all ρ. Our model is, of course, not in a steady state, as there is a positive basin-integrated surface density flux $D_{surf}(\rho_{min}) = D_{net}(\rho_{min})$. This density flux passes almost unchanged [see the nearly uniform values of $D_{net}(\rho)$] through the lighter ($\sigma < 27$) extended isopycnals—these *are* almost in steady state—and is absorbed within the heavier ($\sigma > 27$) isopycnals, so making the water within them more dense.

The ''true'' water mass formation rate M_{true} (the thick full line in Fig. 10c) is found from the volume changes of density layers (see the appendix). It is then integrated to give the true transformation rate G_{true} (the thick full line in Fig. 10b) and once more to give the implied diapycnal density flux D_{true} in Fig. 10a. Agreement with D_{net} is reassuringly good over the resolved isopycnals, $\sigma > 25.65$, but is poorer for the lighter waters, presumably as a result of sampling problems over the small volumes of these waters.

The increase in density of waters $\sigma > 27$ resulting from the absorption of the net density flux is evident in the plot of G_{true} in Fig. 10b. The transformation rate reaches a maximum of $\sim$7 Sv at $\sigma \approx 27.6$. This drives (Fig. 10b) an overall formation of the densest waters, $\sigma > 27.6$, at the expense of thermocline and intermediate waters, $26.5 < \sigma < 27.6$; this is attempting to mimic the formation and export of North Atlantic Deep Water within the real ocean.

Over the whole basin, mixing almost balances surface forcing, and the model is nearer the steady state $D_{surf} = -D_{diff}$ (section 2c) than the direct water mass formation balance $G_{true} = F = -\partial D_{surf}/\partial\rho$ (section 2b). The true transformation and formation rates G_{true} and M_{true} (the thick lines in Figs. 10b and 10c) are very different from those (the dotted lines) implied by surface forcing.

c. The relative importance of mixing processes

We now investigate the relative importance of the various components of mixing in the model Atlantic. As in section 3, the interior diffusion is separated into

$$D_{diff} = D_{lat} + D_{ent} + D_{thermo},$$

where D_{lat} is the basin-integrated lateral mixing in the mixed layer, D_{ent} is the basin-integrated entrainment mixing immediately beneath the mixed layer, and D_{thermo} is the basin-integrated diapycnal diffusion within the thermocline proper. We further separate the entrainment mixing D_{ent} into that which occurs with the seasonal cycle, D_{seas}, and through sustained tropical upwelling, D_{equat}:

$$D_{ent} = D_{seas} + D_{equat}. \quad (31)$$

Here $D_{seas}(\rho)$ is diagnosed as the entrainment flux integrated over that area that both (i) lies north of the winter outcrop line for that ρ (to ensure that the flux *is* associated with the seasonal cycle) and (ii) lies north of a line lying from Florida to West Africa, at approximately 24°N (to ensure that the mixed layer depth varies seasonally).

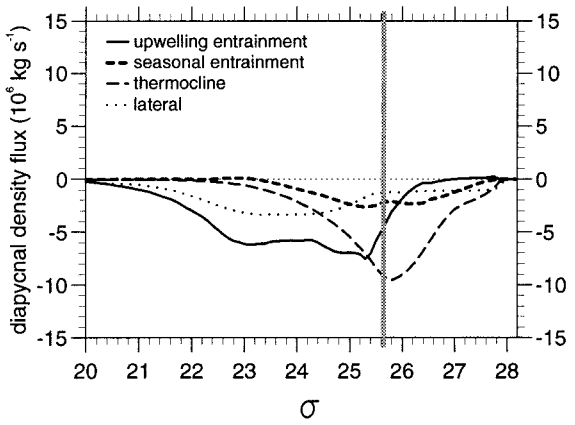

FIG. 12. Annual-mean basin-integrated interior diffusive flux D_{diff} separated into explicit thermocline diffusion D_{thermo} (thin dashed line), the entrainment flux from equatorial and eastern boundary upwelling regions D_{equat} (full line), the entrainment flux in the seasonal boundary layer D_{seas} (thick dashed line), and the horizontal diffusive flux within the mixed layer D_{lat} (dotted line). Units are 10^6 kg s^{-1}.

These components of D_{diff} are shown as functions of ρ in Fig. 12. The largest components of D_{diff} are from the diapycnal mixing D_{thermo} and equatorial upwelling D_{equat}. These terms represents a key part of the oceanic density balance: the return path of the thermohaline circulation. Dense water formed by surface cooling at high latitudes is warmed and lightened as it upwells in the Tropics. Most of the mixing due to equatorial upwelling of the light waters $\sigma < 25.65$ that are not resolved by the model is accomplished by entrainment. Lateral diffusion and seasonal entrainment are comparatively unimportant over the whole model domain.

d. The spatial variation of diffusive fluxes

We now investigate *where* the density fluxes across isopycnals occur in our model. We consider two of the lighter isopycnals in the model thermocline, $\sigma = 26.55$ and $\sigma = 25.8$. We choose $\sigma = 26.55$ in particular to show where seasonal mixing is important and $\sigma = 25.8$ to show equatorial entrainment.

1) THE $\sigma = 26.55$ ISOPYCNAL

The annual averages of each of the diffusive fluxes per unit horizontal area through the $\sigma = 26.55$ surface are shown in Fig. 13; the gray area denotes where a diffusive flux does not exist. The winter and summer outcrops are marked in Fig. 13 by the boundary of the gray shading to the south and the thick dash–dotted line to the north, respectively.

The surface flux per unit area $\mathcal{D}_{surf}$ in Fig. 13a shows generally positive values of $\sim 10^{-6}$ kg s^{-1} m^{-2} [$\sim$17 W m^{-2}] representing an oceanic density gain. Oceanic density loss is confined to isolated near-coastal regions.

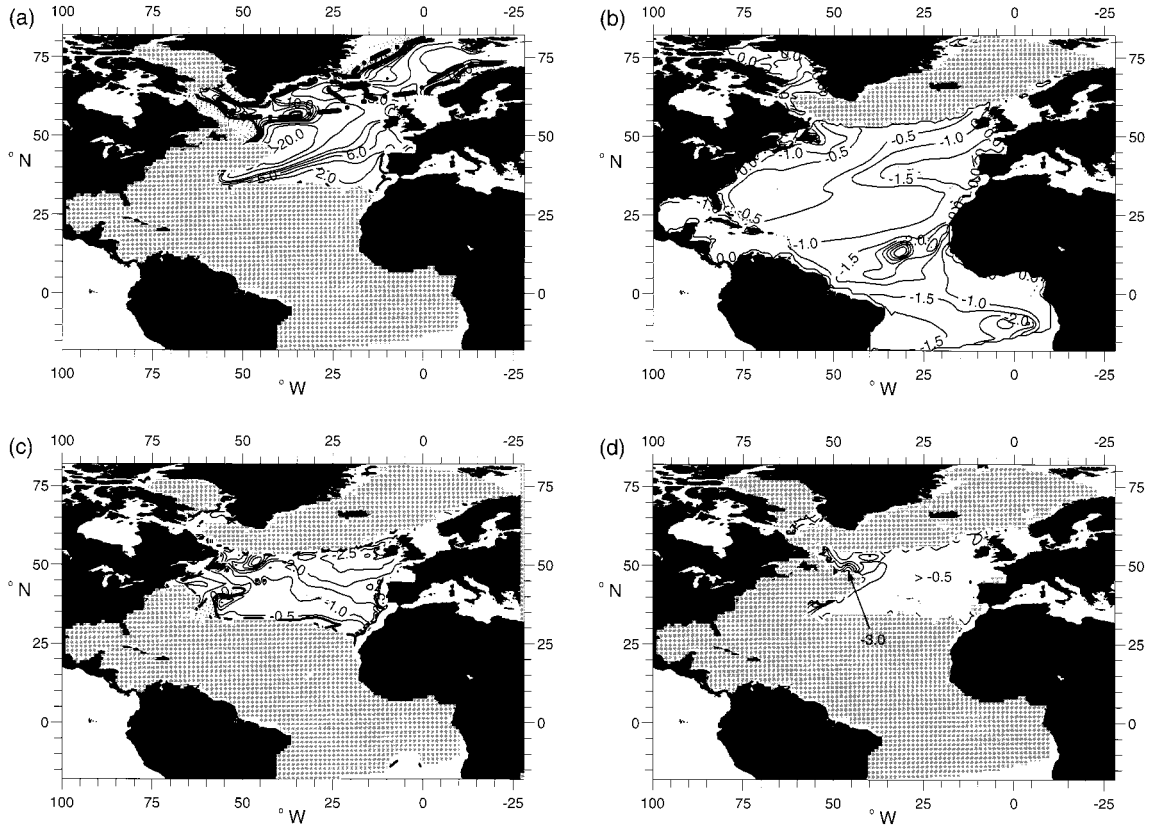

FIG. 13. The annual-average diapycnal density flux per unit area across $\sigma = 26.55$ for (a) surface flux $\mathcal{D}_{surf}$, (b) explicit diapycnal flux $\mathcal{D}_{thermo}$, (c) entrainment flux $\mathcal{D}_{ent}$, and (d) the horizontal diffusive flux within the mixed layer $\mathcal{D}_{lat}$. Positive contours are solid, negative contours dotted for $\mathcal{D}_{surf}$, and vice versa (for clarity) for $\mathcal{D}_{ent}$, $\mathcal{D}_{thermo}$, and $\mathcal{D}_{lat}$. In each case, the shaded areas denote regions where the surface does not exist in the form appropriate to the forcing. The summer and winter outcrops in (a) are marked by the dashed–dotted line and the start of the grayed area, respectively. Units are 10^{-7} kg s^{-1} m^{-2}. C.I. is 0.5 in (b)–(d) and contours at 0, ± 2, ± 4, ± 6, ± 8, ± 10, ± 15, and ± 20 in (a).

The diapycnal density flux, $\mathcal{D}_{thermo} = \kappa_d \partial\rho/\partial z$, is plotted in Fig. 13b. Values are typically $\sim -1 \times 10^{-7}$ kg s^{-1} m^{-2}. Since the diffusion coefficient [Eq. (28)] is proportional to the reciprocal of the buoyancy frequency, N^{-1}, the density flux is proportional to N. Fluxes are weak over the weakly stratified mode waters of the western North Atlantic, but stronger in the strongly stratified equatorial thermocline.

The entrainment density flux, $\mathcal{D}_{ent}$ in Fig. 13c, is on this surface associated with the seasonal cycle of mixed layer deepening and shoaling as seen at OWS Papa in Fig. 1. Typical values are -1 to -2 ($\times 10^{-7}$ kg s^{-1} m^{-2}), similar in magnitude to those of $\mathcal{D}_{thermo}$. However, they exist over a smaller area and so in an integrated sense are less important.

The lateral density flux at any instant is restricted to the isopycnal's outcrop in the mixed layer, so the field $\mathcal{D}_{lat}$ in Fig. 13d gives a ''smeared out'' picture of the outcrop as it moves northward and southward over the year. Typical values are -1 to -2 ($\times 10^{-8}$ kg s^{-1} m^{-2}), but reach -4×10^{-7} kg s^{-1} m^{-2} [~ 7 W m^{-2}] along the flank of the model Labrador Current, where the winter mixed layer is deep and density gradients are strong.

2) THE $\sigma = 25.8$ ISOPYCNAL

Fluxes through this lighter isopycnal are plotted in Figs. 14a–d. They are broadly similar to those on $\sigma = 26.55$, but show important differences. Obviously, because the isopycnal is lighter, it outcrops farther south, so there is a larger area (Fig. 14a) over which there is a $\mathcal{D}_{surf}$. This surface is close to the tropical mixed layer and has a stronger stratification across it, resulting (Fig. 14b) in stronger $\mathcal{D}_{thermo}$. This is, of course, necessitated by the need to balance the much stronger D_{surf} resulting from the more southerly outcrop.

Entrainment is also stronger, (Fig. 14c), with entrainment in the Tropics as well as the seasonal entrainment evident between the winter and summer outcrop lines. Lateral mixing, on the other hand, is weaker than on $\sigma = 26.55$ because the winter mixed layer is less deep at this density. It is strongest along the winter outcrop line where the isopycnal remains almost stationary for a few months.

e. Extratropical balances

We now consider whether there are geographical regions of the model in which Speer and Tziperman's

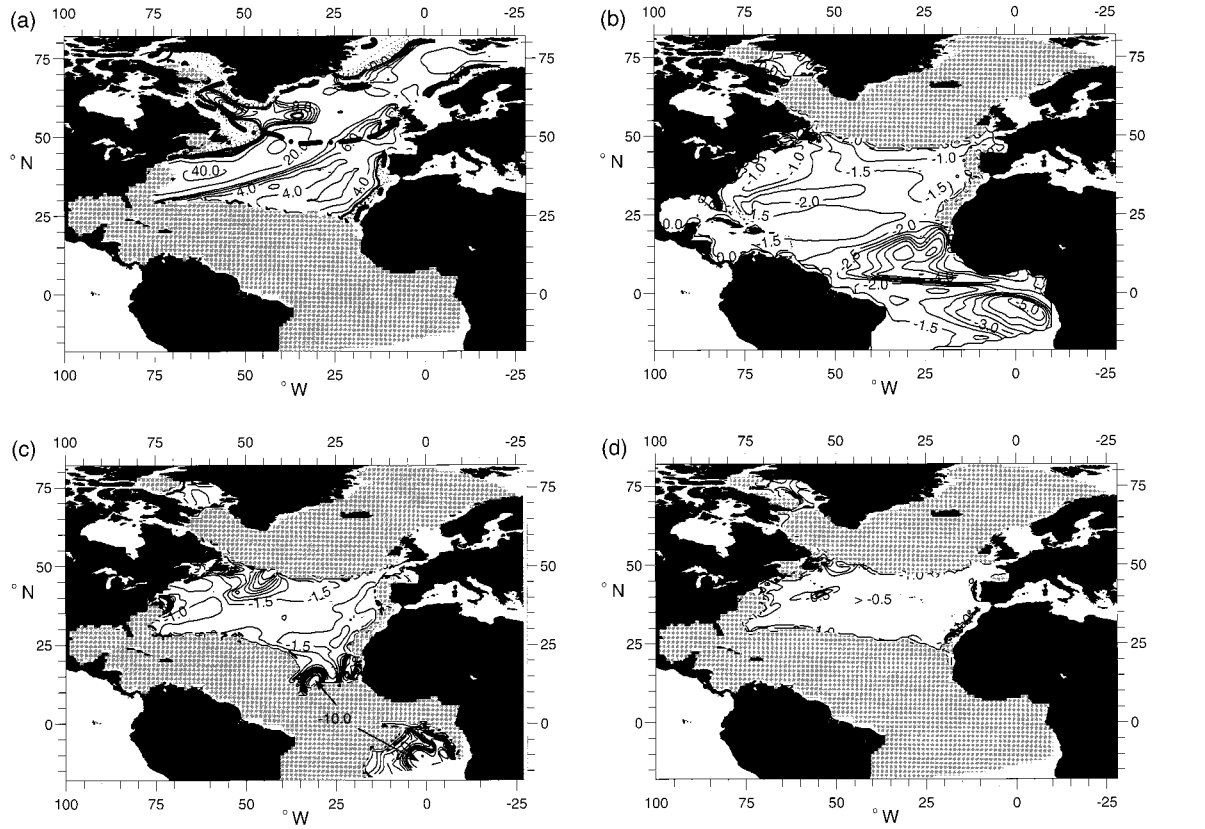

FIG. 14. The annual-average diapycnal density flux per unit area across $\sigma = 25.8$ for (a) surface flux $\mathcal{D}_{surf}$, (b) explicit diapycnal flux $\mathcal{D}_{thermo}$, (c) entrainment flux $\mathcal{D}_{ent}$, and (d) the horizontal diffusive flux within the mixed layer $\mathcal{D}_{lat}$. Units, contour styles, and C.I. as in (14), except in (b) contours also at -6, -8, -10, and -20.

(1992) technique of diagnosing diapycnal volume fluxes directly from the surface forcing might give reasonable results.

Since mixing is evidently strongest over the equatorial regions (see, e.g., Fig. 14), we now diagnose the model north of a nominal line of 24°N; the actual line follows a coordinate line in the rotated model grid. The model ought also to be more realistic over this subdomain than over the whole domain, as (i) the effect of the closed southern boundary should be less and (ii) the unresolved waters with $\sigma < 25.65$ are less important north of 24°N.

In Fig. 15a we plot D_{surf}, D_{diff}, D_{net}, and D_{true} diagnosed north of 24°N, similarly to the globally diagnosed values in Fig. 10a. In Fig. 15b we plot similarly F, G_{diff}, G_{true}, and the residual $G_{true} - F$.

Over this more restricted region, there is a much improved correspondence between F and G_{true}. Thus, surface forcing does provide a reasonable first-order estimate of the diapycnal volume flux outside of the Tropics. Consistent with this, mixing is much weaker than it was over the whole domain, with a peak magnitude of $D_{diff} \sim 4 \times 10^6$ kg s^{-1} compared with the peak of $\sim 20 \times 10^6$ kg s^{-1} over the whole domain. Density is being input into all isopycnals (see the plot of F, the dotted line in Fig. 15b). The domain-integrated density input, $D_{surf}(\sigma_{min})$, is 35×10^6 kg s^{-1}, approximately equivalent to a heat loss over this domain of 0.6 PW. Over this domain, the model is not far from the idealized limit in section 2b with no mixing and density input everywhere.

However, while the broad structure is captured, the surface forcing F predicts (Fig. 15b) a diapycnal volume flux that is too large for waters denser than $\sigma = 25.5$ and too small for lighter waters. For example, $F = 3$ Sv at $\sigma = 25$ and 8 Sv at $\sigma = 26.5$, compared with the true diapycnal volume fluxes of 6 and 5 Sv, respectively. Thus, mixing still plays a significant role.

We again separate the mixing flux (Fig. 16a) into explicit diffusion D_{thermo}, upwelling entrainment D_{equat}, seasonal entrainment D_{seas}, and lateral mixing in the mixed layer D_{lat}. Over this domain, which excludes the tropical upwelling regions, D_{equat} almost disappears, and the thermocline mixing D_{thermo} is much weaker than over the whole domain, with a peak of 2×10^6 kg s^{-1} rather than the peak of 10×10^6 kg s^{-1} seen in Fig. 12. Seasonal entrainment is now of comparable importance, with a peak magnitude of $\sim 2.5 \times 10^6$ kg s^{-1}, in reasonable agreement with the estimate made in section 3d.

The effects of these mixing processes on the diapyc-

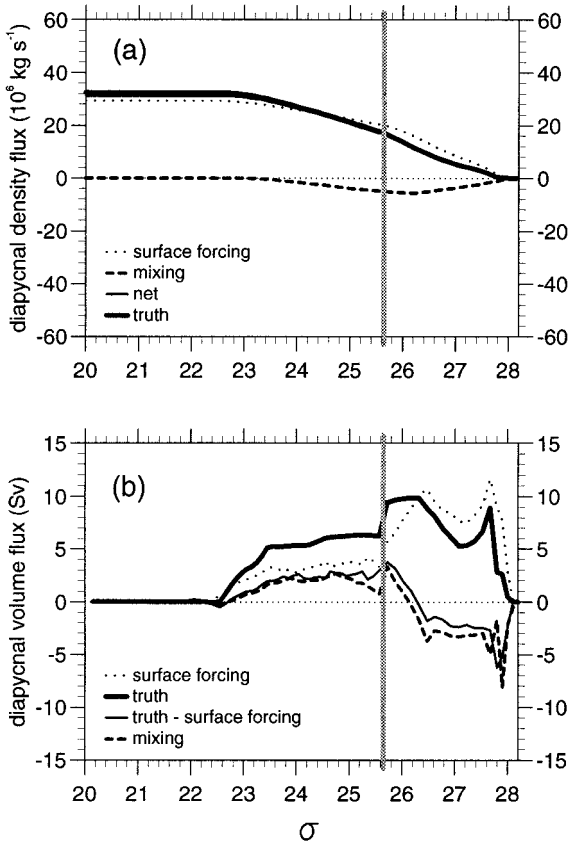

FIG. 15. (a) Diapycnal density fluxes north of 24°N in 10^6 kg s^{-1}. Surface forcing D_{surf}, (dotted line), truth (thick, solid line), mixing D_{diff} (dashed line), and diagnosed D_{net} (thin solid line) not visible as almost coincident with truth. (b) The diapycnal volume flux G north of 24°N estimated from the surface forcing (dotted line) and from model truth (full line). The mismatch between the surface forcing and model truth (thin line) is indeed close to the diagnosed mixing (dashed line). Units in Sv.

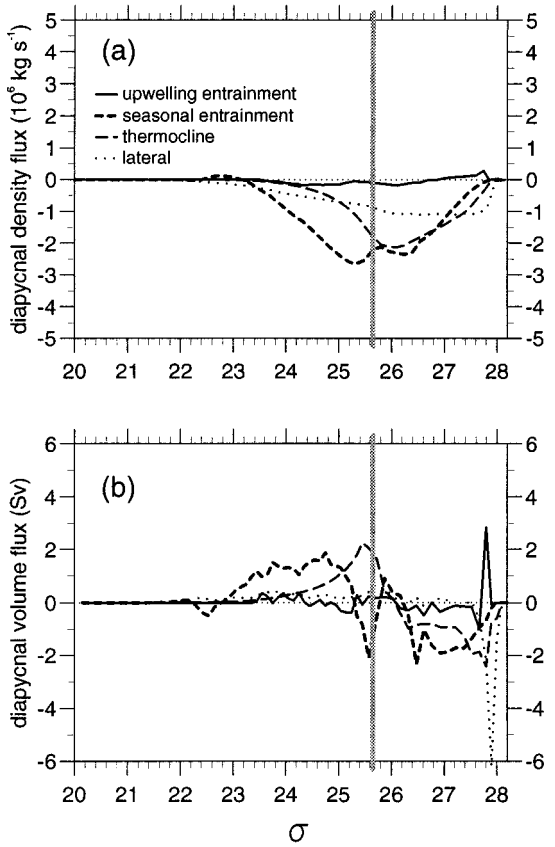

FIG. 16. (a) Diapycnal density fluxes driven by various components of mixing, as in Fig. 12, north of 24°N (10^6 kg s^{-1}). (b) Implied diapycnal volume fluxes driven by various components of mixing (Sv).

nal volume flux are shown in Fig. 16b. Seasonal entrainment drives a volume flux of ~2 Sv from dense to light for the thermocline and intermediate waters, while lateral mixing in the mixed layer drives a flux of ~6 Sv from dense to light for heavy waters $\sigma \approx 27.9$. These processes perhaps ''fine tune'' the properties of the water masses, already approximately set by the surface fluxes.

f. Within localized regions

Speer and Tziperman's (1992) technique of diagnosing diapycnal volume fluxes directly from the surface forcing might be expected to give the best results of all when applied to the formation regions. We thus consider the diagnosed formation rates in the Sargasso and Labrador Seas, where the model forms versions of 18° subtropical mode water and Labrador Sea Water, respectively; the Sargasso Sea is defined here by the region roughly from 24° to 35°N, 70° to 50°W and the Labrador Sea by 53° to 64°N, 55° to 28°W. Over the Sargasso Sea, the surface forcing leads to a formation rate of up to 15 Sv/(kg m^{-3}) at $\sigma = 26.55$, which is close to the model truth revealed by the close correspondence between the dotted and solid lines in Fig. 17a. Over this region, mixing makes a relatively minor contribution, compared with the strength of the surface forcing.

Over the Labrador and Irminger Seas, the surface forcing and model formation rates closely agree, with a formation rate of 35 Sv /(kg m^{-3}) at $\sigma = 27.75$ being compensated by destruction of 30 Sv /(kg m^{-3}) at $\sigma = 27.6$ (Fig. 17b). Again mixing only plays a relatively minor role locally.

g. Implied vertical diffusivity

The underlying appeal of Walin's formulation is not only that rates of water mass formation might be predictable from surface forcing, but also that the integrated mixing might be inferred by comparing air–sea fluxes with known formation rates. This can be either done globally or, if the in- and outflows are known, over restricted domains. Applications using real data have so

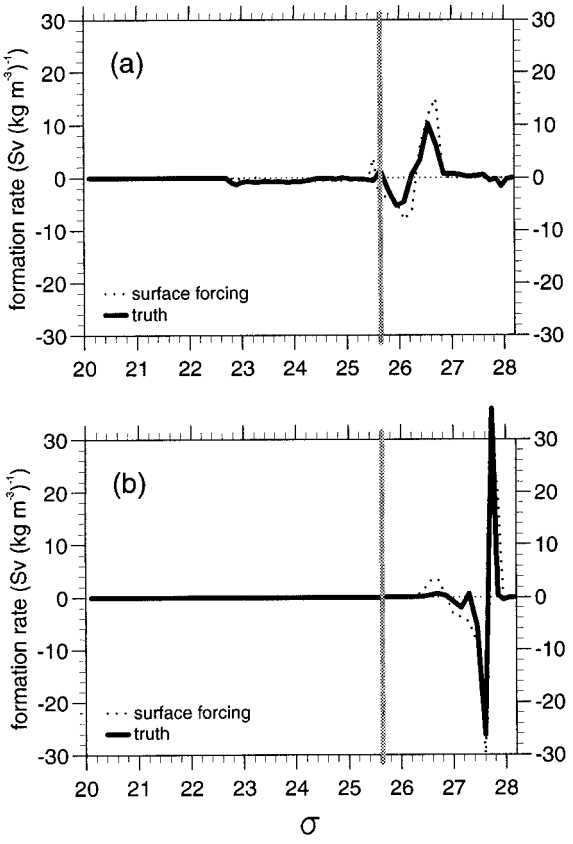

FIG. 17. Annual mean layer formation rates over (a) the Sargasso Sea and (b) the Labrador–Irminger Sea. The contribution from surface forcing $M_{\text{surf}}(\rho_k)$ is denoted by a dotted line and an independent truth $M_{\text{true}}(\rho_k)$ by the thick line. Units are Sv/(kg m^{-3}).

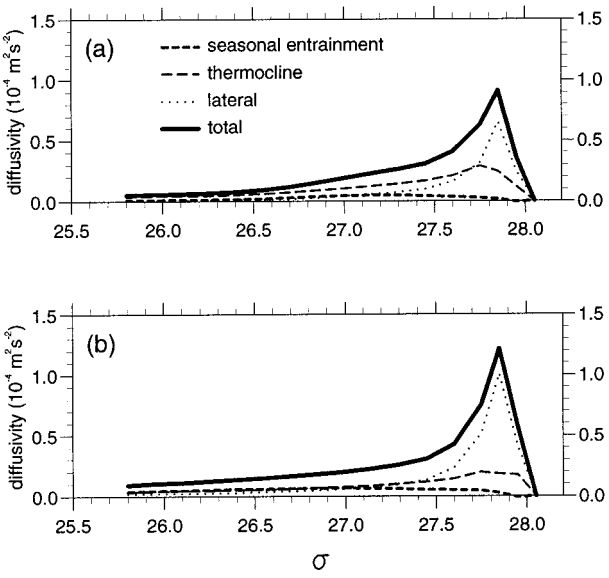

FIG. 18. Implied diffusivities. Thick lines are total implied diffusivity, dotted due to lateral mixing, dashed due to thermocline diffusion, thin full line due to seasonal entrainment. (a) Diagnosed globally and (b) north of 24°N.

far assumed that the (annual mean) ocean is in steady state.

Walin (1982) estimated an implied globally averaged vertical diffusivity in the ocean to be 2×10^{-4} m^2 s^{-1} using surface fluxes calculated from COADS data by Andersson et el. (1982) and assuming a background uniform $\partial T/\partial z = 4 \times 10^{-3}$ K m^{-1}. This diffusivity estimate is an order of magnitude larger than the canonical value for the thermocline of $\sim 2 \times 10^{-5}$ m^2 s^{-1} found by Ledwell et al. (1993). This discrepancy between the global diffusivity inferred from integrated tracer diagnostics and local measurements is undoubtedly the result of mixing being strongly enhanced in some regions. Speer (1997) estimated the effective diffusivity as a function of density over the North Atlantic by comparing the volume flux along density layers across a hydrographic section at 11°S with the formation rates implied from climatological forcing north of there. The implied diffusivity ranges from 10^{-4} m^2 s^{-1} at $\sigma = 23$ to lower values varying around 2×10^{-5} m^2 s^{-1} for denser surfaces.

We now apply this diagnostic approach to our model. We diagnose an effective diffusivity based on the traditional assumption that mixing only occurs within the thermocline, even though mixing is really also occurring within the mixed layer (through lateral mixing) and at its base (through entrainment). This effective diffusivity $\kappa_{\text{eff}}(\rho)$ is then the total diffusive flux across the isopycnal D_{diff}, divided by the density gradient, integrated over the area $\mathcal{A}_{\text{thermo}}$ of the isopycnal where it lies within the thermocline:

$$\kappa_{\text{eff}}(\rho) = \frac{\langle D_{\text{diff}}(\rho) \rangle}{\left\langle \int_{\mathcal{A}_{\text{thermo}}(\rho,t)} \frac{\partial \rho}{\partial z}\, dA \right\rangle}. \tag{32}$$

The brackets are explicitly included to emphasize that annual means of these quantities are taken.[2]

We calculate effective diffusivities both over the whole model domain and over the extratropical domain north of 24°N.

Over the full domain, the variation of effective diffusivity with density over the model density range that is resolved in the thermocline, $25.65 < \sigma < 28.15$, is shown as the thick full line in Fig. 18a. Values range from $\sim 0.1 \times 10^{-4}$ m^2 s^{-1} at $\sigma < 26.0$ to $\sim 0.9 \times 10^{-4}$ m^2 s^{-1} at $\sigma = 27.85$, about three times the explicit diapycnal diffusivity, itself fairly large at this density

[2] The density gradient is calculated as the difference in density between two layers divided by the distance between their midpoints, even when the lighter layer is the mixed layer. This is how it is calculated in evaluating explicit diapycnal diffusive fluxes in (28). This implies a finite density gradient for density surfaces too light ($\sigma < 25.65$) to be resolved in the model.

(28) because of the low N in these weakly stratified subpolar mode waters. This enhancement at high densities results from lateral mixing within the deep winter mixed layers. Seasonal entrainment begins to dominate over lateral mixing for $\sigma < 27$, as is seen better in Fig. 12, but at these lighter densities the explicit diapycnal diffusion dominates anyway (again see Fig. 12). However, the lateral and seasonal mixing do increase the diffusivity by about a half over the explicit diffusion for the mid to deep thermocline waters, $26.6 < \sigma < 27.4$.

North of 24°N (Fig. 18b), the effective diffusivity shows a similar pattern of variation with ρ. Values of κ_{eff} are however larger, with the peak at $\sigma = 27.85$ now reaching $\sim 1.3 \times 10^{-4}$ m^2 s^{-1}. Excluding the tropical mixing, which is driven by the strong density gradients under the tropical mixed layer, and hence is associated with *weak* diffusivity (28), gives a larger effective diffusivity for the remainder of the mixing. Moreover, the seasonal entrainment and lateral mixing are then relatively more important (see again the diffusive fluxes in Fig. 16a) and so increase κ_{eff} more.

5. Discussion

Walin (1982) proposed that the ocean circulation should be understood in terms of the movement of water across isotherms (here isopycnals). Using his formulation, the volume between two isopycnals over a closed domain is only conserved if either there is no integrated air–sea forcing or the air–sea forcing is balanced by diffusion. Since climatologies show that the air–sea forcing does not in general integrate to zero between two isopycnals, then clearly diffusion must be important in obtaining a closed, steady circulation over the ocean.

In our study, we diagnose the transfer of water masses across isopycnals using the Walin formulation applied to output from a seasonally varying, non-eddy-resolving,[3] simulation of the North Atlantic using an isopycnic model. Diagnostics show that the air–sea forcing is attempting to *increase* the contrast in water masses across the basin, while mixing is attempting to *reduce* this contrast. Within the model, there is an approximate balance between air–sea forcing and mixing over the whole domain, although this balance does not hold locally.

The modeled North Atlantic thermohaline circulation is closed for surface and intermediate waters, but still involves an overall formation of dense waters. Dense waters ($\sigma > 27.6$) are formed more rapidly by surface density gain at high latitudes, than they are destroyed by mixing—in reality these waters are exported from the North Atlantic and lightened elsewhere in the World Ocean. Intermediate waters ($27.0 < \sigma < 27.6$) are formed in the northern North Atlantic by surface forcing and consumed by strong mixing in upwelling regions in the Tropics and eastern boundary within an advective/diffusive boundary layer of O(50 m) depth; McWilliams et al. (1996) found a similar result in a z coordinate GCM. While the density transfer through this boundary layer is *achieved* by diffusion, this density transfer is *driven* by the upward motion of dense waters into the light mixed layer. Indeed, in a separate model run without diapycnal mixing all of this conversion of dense waters to light mixed layer waters was achieved by entrainment. Hence there is no need for interior mixing to close the circulation of intermediate waters. Interior mixing merely sets the density structure of the equatorial upwelling waters.

Outside the upwelling regions, mixing occurs through entrainment within the seasonal boundary layer and lateral mixing within the mixed layer. The seasonal entrainment is relatively important for isopycnals with summer and winter outcrops that are widely separated, whereas lateral mixing is important for denser isopycnals outcropping in the subpolar gyre where the mixed layer is thick. Each of these mixing processes drive volume fluxes that attain 4–5 Sv, compared with the volume flux driven by air–sea fluxes of ~12 Sv. Therefore, a crude, first-order estimate of the formation rate of water masses may be made solely from the air–sea fluxes (as advocated by Speer and Tzipermann 1992), but this estimate is improved by taking into account the mixing within the seasonal boundary layer.

Walin's approach can be used to estimate the integrated mixing, either globally or over restricted regions, by comparing the air–sea forcing with the in- and outflows of particular density classes through hydrographic sections bounding the domain, as recently applied by Speer (1997). In our model, the effective diffusivity is found to result from enhanced mixing in special regions, rather than reflecting a background spatially uniform value. Indeed, it is found to vary more strongly with density than does the actual diffusive flux.

As mixing must always act to reduce density contrasts across the domain, such comparisons of water mass formation predicted from surface fluxes with actual water mass export across hydrographic sections may give extra constraints that can expose deficiencies in surface flux climatologies.

Acknowledgments. This work has been carried with the support of the United Kingdom Ministry of Defence. RGW is grateful for support from the NERC UK WOCE Special Topic fund GST/02/813. The version of MICOM used here was set up with the assistance of Yanli Jia and Adrian New.

[3] While this GCM does not resolve eddies, the diagnostic approach of Walin (1982) still holds in their presence, as has been pointed out by Marshall (1997) who emphasizes the connection with the eddy-driven subduction and total transport of tracers.

APPENDIX

Evaluation of the Model Diapycnal Fluxes

In the following discretizations, each model layer k has a prescribed density ρ_k, and the mixed layer density at each gridpoint i, j (on the rotated grid) at timestep n is written as $\rho^n_{m,i,j}$. To achieve the highest possible accuracy, we determine annual-mean fluxes by online time integration over model year 31.

a. Vertical discretization of diffusive fluxes, diapycnal volume fluxes, and formation rates

We define diffusive fluxes and formation rates at layer densities ρ_k, but diapycnal volume fluxes at interface densities $\rho_{k-1/2}$. Hence

$$G(\rho_{k-(1/2)}) = -\frac{D_{\text{net}}(\rho_k) - D_{\text{net}}(\rho_{k-1})}{\rho_k - \rho_{k-1}}. \quad \text{(A1)}$$

The formation rate of layer k, $M(\rho_k)$, simply follows as

$$M(\rho_k) = -\frac{G(\rho_{k+(1/2)}) - G(\rho_{k-(1/2)})}{\rho_{k+(1/2)} - \rho_{k-(1/2)}}. \quad \text{(A2)}$$

b. Model truth

For layer k we determine a true water mass formation rate $M_{\text{true}}(\rho_k)$ from changes in regionally integrated layer volume (including mixed layer water, classified by layer density ranges), taking into account any advective and diffusive volume fluxes across any open boundaries (which are defined as positive out of the domain).

We can further derive $G_{\text{true}}(\rho_{k-1/2})$ and $D_{\text{true}}(\rho_k)$ by integrating $M_{\text{true}}(\rho_k)$ with respect to ρ_k.

c. Surface diapycnal flux

The annual-mean surface diapycnal flux is given by (30). In the model we discretize this as

$$D_{\text{surf}}(\rho) = \frac{1}{\tau_{\text{year}}} \sum_{n=1}^{N} \Delta t \sum_{i,j} A_{i,j} h^n_{m,i,j} \Delta\rho^n_{m,i,j} \Pi_{\text{surf}}(\rho, \rho^n_{m,i,j}), \quad \text{(A3)}$$

where $h^n_{m,i,j}$ is the mixed layer depth, $\Delta\rho^n_{m,i,j}$ is the change in mixed layer density due to the net surface density flux applied at time step n, $A_{i,j}$ is surface area represented by a gridpoint, N is the number of time steps per year (where each time step, $\Delta t = 48$ min), and $\Pi_{\text{surf}}(\rho, \rho^n_{m,i,j})$ is a sampling function: $\Pi_{\text{surf}} = 1$ if $\rho < \rho^n_{m,i,j}$.

The thermal and haline fluxes are set to zero wherever model or climatological sea surface temperature falls below -1.8°C, as in New et al. (1995).

d. Diapycnal entrainment fluxes

In the model we compute the annual average of the basin-integrated entrainment flux (20) as

$$\langle D_{\text{ent}}(\rho)\rangle = -\frac{1}{\tau_{\text{year}}} \sum_{n=1}^{N} \Delta t \sum_{i,j} A_{ij} \sum_{k=2}^{20} s^n_{i,j,k} (\rho_k - \rho) \Pi_{\text{ent}}(\rho, \rho^n_{m,i,j}, \rho_k), \quad \text{(A4)}$$

where $s^n_{i,j,k}$ is the entrainment velocity between the mixed layer and layer k at time step n, and $\Pi_{\text{ent}}(\rho, \rho^n_{m,i,j}, \rho_k)$ is a sampling function: $\Pi_{\text{ent}} = 1$ if $\rho^n_{m,i,j} < \rho < \rho_k$—that is, Π_{ent} samples the entrainment density flux across isopycnals lying in the ''bundle'' at the base of the mixed layer.

e. Interior diffusive flux

In version 2.4 of MICOM, a diapycnal velocity due to diapycnal mixing, $e_{k+1/2}$, across the interface between layers k and $k + 1$, is defined by Hu (1996) as

$$e_{k+(1/2)} = \frac{\left(\kappa_d \frac{\partial\rho}{\partial z}\right)_k - \left(\kappa_d \frac{\partial\rho}{\partial z}\right)_{k+1}}{\rho_k - \rho_{k+1}}, \quad \text{(A5)}$$

where κ_d is parameterized here as $\kappa_d = c/N$, with $c = 0.575 \times 10^{-7}$ m^2 s^{-2}, and N is the buoyancy frequency.

As the interior diapycnal mixing is thus represented by interfacial mass fluxes, we obtain $\langle D_{\text{thermo}}(\rho)\rangle$, the annual average of the basin-integrated diffusive flux (26) by integrating the diapycnal volume flux $\langle G_{\text{thermo}}(\rho)\rangle$ with respect to ρ, where

$$\langle G_{\text{thermo}}(\rho)\rangle = -\frac{1}{\tau_{\text{year}}} \sum_{n=1}^{N} \Delta t \sum_{i,j} A_{ij} \left\{ e^n_{m,i,j} \Lambda_1(\rho, \rho^n_{m,i,j}, \rho^n_{kth,i,j}) + \sum_{k=2}^{19} e^n_{i,j,k+(1/2)} \Lambda_2(\rho, \rho_k, \rho_{k+1}) \right\}. \quad \text{(A6)}$$

Here, at time step n, $e^n_{i,j,k+1/2}$ is the vertical velocity representing interior diapycnal mixing across the interface between layer k and layer $k + 1$, and $e^n_{m,i,j}$ is the corresponding velocity across the base of the mixed layer. The sampling function, $\Lambda_1(\rho, \rho^n_{m,i,j}, \rho^n_{kth,i,j}) = 1$ if $\rho^n_{m,i,j} < \rho < \rho^n_{kth,i,j}$, where layer kth is the lightest interior layer of finite thickness;—that is, it samples diapycnal mixing across an isopycnal that lies at the mixed layer base, while $\Lambda_2(\rho, \rho_k, \rho_{k+1}) = 1$ if $\rho_k < \rho < \rho_{k+1}$—that is, it samples mixing between interior layers.

f. Lateral diffusive flux

In the model we compute the annual average of the basin-integrated lateral mixed layer diffusive density flux $D_{\text{lat}}(\rho)$, given in (16), as the sum of lateral diffusive fluxes across the four sidewalls (at $i - \frac{1}{2}$, $j - \frac{1}{2}$, $i + \frac{1}{2}$, and $i + \frac{1}{2}$) of each (i, j) gridbox:

$$D_{\text{lat}}(\rho) = -\frac{1}{\tau_{\text{year}}}\sum_{n=1}^{120}\Delta t\Bigg\{\sum_{i,j}\Delta x_{i,j-(1/2)}h^n_{i,j-(1/2)}\kappa_h\left(\frac{\rho^n_{m,i,j}-\rho^n_{m,i,j-1}}{y_{i,j}-y_{i,j-1}}\right)\Pi(\rho,\,\rho^n_{m,i,j},\,\rho^n_{m,i,j-1})$$
$$-\sum_{i,j}\Delta y_{i-(1/2),j}h^n_{i-(1/2),j}\kappa_h\left(\frac{\rho^n_{m,i,j}-\rho^n_{m,i-1,j}}{x_{i,j}-x_{i-1,j}}\right)\Pi(\rho,\,\rho^n_{m,i,j},\,\rho^n_{m,i-1,j})$$
$$-\sum_{i,j}\Delta x_{i,j+(1/2)}h^n_{i,j+(1/2)}\kappa_h\left(\frac{\rho^n_{m,i,j+1}-\rho^n_{m,i,j}}{x_{i,j}-x_{i-1,j}}\right)\Pi(\rho,\,\rho^n_{m,i,j},\,\rho^n_{m,i,j+1})$$
$$-\sum_{i,j}\Delta y_{i+(1/2),j}h^n_{i+(1/2),j}\kappa_h\left(\frac{\rho^n_{m,i+1,j}-\rho^n_{m,i,j}}{x_{i,j}-x_{i-1,j}}\right)\Pi(\rho,\,\rho^n_{m,i,j},\,\rho^n_{m,i+1,j})\Bigg\}, \tag{A7}$$

where Δx and Δy are lengths of east–west and north–south sidewalls, respectively, and $\Pi(\rho,\,\rho^n_{m,i,j},\,\rho^n_{m,i-1,j})$ is a sampling function, taking the value 1 for $\rho^n_{m,i,j} < \rho < \rho^n_{m,i-1,j}$, otherwise 0. Here κ_h is typically 10^3 m^2 s^{-1}, being dependent on variable grid resolution ($\kappa_h = u_d L$, where $u_d = 10^{-2}$ m s^{-1} is a diffusion velocity for temperature, and L is the length of a gridcell wall across which temperature diffuses).

REFERENCES

Armi, L., 1978: Some evidence for boundary mixing in the deep ocean. *J. Geophys. Res.,* **83,** 1971–1979.

Bleck, R., H. P. Hanson, D. Hu, and E. B. Krauss, 1989: Mixed layer thermocline interaction in a three-dimensional isopycnic coordinate model. *J. Phys. Oceanogr.,* **19,** 1417–1439.

——, C. Rooth, D. Hu, and L. T. Smith, 1992: Salinity-driven thermocline transients in a wind- and thermohaline-forced isopycnic coordinate model of the North Atlantic. *J. Phys. Oceanogr.,* **22,** 1486–1505.

Brainerd, K. E., and M. C. Gregg, 1996: Surface mixed and mixing layer depths. *Deep-Sea Res.,* **42,** 1521–1543.

Bryden, H. L., and E. C. Brady, 1985: Diagnostic model of the three-dimensional circulation in the upper equatorial Pacific Ocean. *J. Phys. Oceanogr.,* **15,** 1255–1273.

Caldwell, D. R., and J. M. Moum, 1995: Turbulence and mixing in the ocean. *Rev. Geophys.,* (Suppl.) *U. S. National Report to IUGG 1991–1994,* 1385–1394.

Esbensen, S. K., and Y. Kushnir, 1981: The heat budget of the global ocean: An atlas based on estimates from surface marine observations. Oregon State University Climate Research Institute Rep. 29, 27 pp.

Garrett, C., and A. Tandon, 1997: The effects on water mass formation of surface mixed layer time-dependence and entrainment fluxes. *Deep-Sea Res.,* **44,** 1991–2006.

Gill, A. E., and P. P. Niiler, 1973: The theory of the seasonal variability in the ocean. *Deep-Sea Res.,* **20,** 141–177.

Haine, T. W. N., and J. C. Marshall, 1998: Gravitational, symmetric, and baroclinic instability of the ocean mixed layer. *J. Phys. Oceanogr.,* **28,** 639–658.

Haney, R. L., 1971: Surface thermal boundary conditions for ocean circulation models. *J. Phys. Oceanogr.,* **1,** 241–248.

Hellerman, S., and M. Rosenstein, 1983: Normal monthly wind stress over the world ocean with error estimates. *J. Phys. Oceanogr.,* **13,** 1093–1104.

Hu, D., 1996: The computation of diapycnic diffusivity and advective scalar fluxes in multilayer isopycnic-coordinate ocean models. *Mon. Wea. Rev.,* **124,** 1834–1851.

Isemer, H. J., and L. Hasse, 1987: *The Bunker Climate Atlas of the North Atlantic Ocean.* Vol. 2, *Air–Sea Interactions,* Springer-Verlag, 218 pp.

Jaeger, L., 1976: Monatskarten des Niedersclags fur die ganze Erde. *Ber. Dtsche. Welterdienstes,* Heft 18, No. 139, Oftenbach, Germany.

Large, W. G., J. C. McWilliams, and S. C. Doney, 1994: Oceanic vertical mixing. A review and a model with a nonlocal boundary layer parameterization. *Rev. Geophys.,* **32,** 363–403.

Ledwell, J. R., A. J. Watson, and C. S. Law, 1993: Evidence for slow mixing across the pycnocline from an open-ocean tracer-release experiment. *Nature,* **364,** 701–703.

Levitus, S., 1982: *Climatological Atlas of the World Ocean.* NOAA Prof. Paper No. 13, U.S. Govt. Printing Office, 173 pp.

Marshall, D. P., 1997: Subduction of water masses in an eddying ocean. *J. Mar. Res.,* **55,** 201–222.

Marshall, J. C., D. Jamous, and J. Nilson, 1998: Reconciling 'thermodynamic' and 'dynamic' methods of computation of water-mass tansformation rates. *Deep-Sea Res,* **46,** 545–572.

McDougall, T. J., 1984: The relative roles of diapycnal and isopycnal mixing on subsurface water mass conversion. *J. Phys. Oceanogr.,* **14,** 1577–1589.

McWilliams, J. C., G. Danabasoglu, and P. R. Gent, 1996: Tracer budgets in the warm water sphere. *Tellus,* **48,** 179–192.

New, A. L., R. Bleck, Y. Jia, R. Marsh, M. Huddleston, and S. Barnard, 1995: An isopycnic model simulation of the North Atlantic Ocean. Part I: Model experiment. *J. Phys. Oceanogr.,* **25,** 2667–2699.

Peters, H., M. C. Gregg, and J. M. Toole, 1988: On the parameterization of equatorial turbulence. *J. Geophys. Res.,* **93,** 1199–1218.

Polzin, K. L., K. G. Speer, J. M. Toole, and R. W. Schmitt, 1995: Intense mixing of Antarctic Bottom Water in the equatorial Atlantic Ocean. *Nature,* **380,** 54–57.

Speer, K. G., 1993: Conversion among North Atlantic surface water types. *Tellus,* **45A,** 72–79.

——, 1997: A note on average cross-isopycnal mixing in the North Atlantic Ocean. *Deep-Sea Res.,* **44,** 1981–1990.

——, and E. Tziperman, 1992: Rates of water mass formation in the North Atlantic Ocean. *J. Phys. Oceanogr.,* **22,** 93–104.

——, H.-J. Isemer, and A. Biastoch, 1995: Water mass formation from revised COADS data. *J. Phys. Oceanogr.,* **25,** 2444–2457.

——, S. R. Rintoul, and B. Sloyan, 1997: Subantarctic Mode Water formation by air-sea fluxes. *Int. WOCE Newslett.,* **29,** 29–31.

Tandon, A., and C. Garrett, 1997: Water mass formation from thermodynamics: A framework for examining compatibility with dynamics. *Int. WOCE Newslett.,* **28,** 34–36.

Toole, J. M., K. L. Polzin, and R. W. Schmitt, 1994: New estimates of diapycnal mixing in the abyssal ocean. *Science,* **264,** 1120–1123.

Tziperman, E., and K. G. Speer, 1994: A study of water mass transformation in the Mediterranean Sea: Analysis of climatological data and a simple 3-box model. *Dyn. Atmos. Oceans,* **21,** 53–82.

Walin, G., 1982: On the relation between sea-surface heat flow and thermal circulation in the ocean. *Tellus,* **34,** 187–195.

Worthington, L. V., 1976: *On the North Atlantic Circulation.* Vol. 6, *John Hopkins Oceanographic Studies,* The John Hopkins University Press, 110 pp.

——, 1981: The water masses of the world ocean: Some results of a fine-scale census. *Evolution of Physical Oceanography: Scientific Surveys in Honor of Henry Stommel,* B. A. Warren and C. Wunsch. Eds., The MIT Press, 42–69.